TECHNISCHE
UNIVERSITÄT
WIEN

Diplomarbeit

Investigation of polymer and copper degradation under corrosive conditions using LIBS and LA-ICP-MS

Ausgeführt am Institut für

Chemische Technologien und Analytik

der Technischen Universität Wien

unter der Anleitung von

Assoc. Prof. Dr. Andreas Limbeck

durch

Maximilian Mayr

Goethestraße 15

3100, St. Pölten

Wien, am

Datum

Unterschrift

This document is set in Palatino, compiled with pdfLaTeX2e and `Biber`.

The LaTeX template from Karl Voit is based on KOMA script and can be found online: https://github.com/novoid/LaTeX-KOMA-template

Affidavit

I declare that I have authored this thesis independently, that I have not used other than the declared sources/resources, and that I have explicitly indicated all material which has been quoted either literally or by content from the sources used. The text document uploaded to TU Wien University Library (https://www.ub.tuwien.ac.at/eng/) is identical to the present master‘s thesis.

Date

Signature

Acknowledgments

First of all I would like to express my gratitude to my supervisor Andreas Limbeck for giving me the opportunity to conduct my master thesis under his supervision. Additionally I would like to thank all members of KAI who worked with me and KAI in general for the financial support that made this work possible.

I especially want to thank Lukas Brunnbauer who trained me and assisted me not only with all practical difficulties and issues in the lab but also the evaluation and interpretation of the generated data. Also many thanks for the nice discussions we had and the fun time we shared, at lunch, during long measurements or after work - and for the encouraging words, whenever something did not work out the way I wanted it to. It was a pleasure to work with you.

Further thanks go to Silvia Larisegger, who invited me to do this master's thesis and also readily helped me whenever I needed advice.

Thank you very much, Rita Wiesinger, Laura Pagnin and Manfred Schreiner, for your support with my weathering experiments and IR measurements - and for granting me access to your instruments at the Academy of Fine Arts Vienna.

I also want to thank all my fellow students and new friends who accompanied me during the past five years at TU Wien (Vienna University of Technology). Special thanks go to Felix, Felix, Markus and Christoph for the great and productive time we had during our studies. Thanks as well to the rest of the working group - especially to Jakob, for being a great office mate and friend.

I am grateful for the many other friends that played a role in my success at university, simply by the fact, that meeting and spending time with them was the perfect counterweight to my studies.

Last but not least I would like to thank my family for unconditionally supporting me in any possible way and always being there for me.

Abstract

Polymers are used in the coating industry as protective layers for many materials. For certain applications the polymer must withstand and protect the underlying material from harsh environmental conditions such as exposure to UV-radiation and corrosive gases (e.g. SO_2 and H_2S). To provide optimal protective properties, the polymer should not degrade under these conditions and should prevent alteration of the underlying material.

One aim of this study was to test LIBS (Laser Induced Breakdown Spectroscopy) and LA-ICP-MS (Laser Ablation Inductively Coupled Plasma Mass Spectrometry) on their feasibility for measurement of polymer degradation and sulfur uptake. Unlike most currently employed techniques, these two are not limited to the surface but also enable depth profiling.

Five different polyimide films on silicon substrate as well as pure copper were weathered in different corrosive atmospheres (50 ppm of SO_2 or H_2S for $\leq$192 h) and then analyzed using LIBS and LA-ICP-MS. Additionally polyimide samples were put in a UV chamber and exposed to UV irradiation for $\leq$96 h.

Using LIBS in combination with multivariate statistics, changes in the polyimide due to UV alteration were successfully observed. Additionally, changes in chemical composition due to the formation of corrosion products on pure copper were analyzed and proved that H_2S is more corrosive than SO_2.

LA-ICP-MS was optimized for the qualitative measurement of gas permeability into the polyimide. The acquisition of depth profiles was successful. It was found that SO_2 weathering results in a significant increase in sulfur signal intensity. The observed increase was strongest in the upper part of the polyimde film and decreased towards the substrate. The H_2S weathering hardly showed a measurable change at all. For two of the five polyimides UV exposure prior to H_2S weathering lead to an increase in sulfur signal in the upper layers of the polymer film.

LIBS and LA-ICP-MS have successfully been employed for measurement of polymer degradation and diffusion in polymers. The findings suggest that SO_2 permeates polyimides more easily than H_2S and that UV exposure significantly influences the permeability and leads to observable degradation of the polyimide.

Kurzfassung

Polymere werden in vielen Bereichen der Beschichtungsindustrie als Schutzschichten verschiedener Materialien verwendet. Bei bestimmten Anwendungen muss das Polymer schädlichen Umwelteinflüssen, wie beispielsweise UV-Strahlung und korrosiven Gasen (z.B. SO_2 und H_2S), widerstehen und das darunterliegende Material schützen. Um längerfristig optimalen Schutzeigenschaften zu gewähren, sollte das Polymer dabei nicht degradieren und das bedeckte Material vor Alterung schützen.

Ein Ziel dieser Studie war, die Machbarkeit der Messung von Polymerdegradation und Schwefelaufnahme, mittels LIBS (Laserinduzierte Plasmaspektroskopie; engl.: laser-induced breakdown spectroscopy) und LA-ICP-MS (Laserablations-Massenspektrometrie mit induktiv gekoppeltem Plasma), zu testen. Anders als viele heutzutage verwendete Techniken sind diese zwei nicht auf Oberflächenanalyse beschränkt, sondern ermöglichen es auch, Tiefenprofile aufzunehmen.

Fünf verschiedene Polyimid-Filme auf einem Siliziumsubstrat, sowie reines Kupfer, wurden unterschiedlicher korrosiver Umgebung (50 ppm SO_2 oder H_2S für $\leq$192 h) ausgesetzt und danach mit LIBS und LA-ICP-MS analysiert. Zusätzlich wurden Polyimid-Proben in einer UV-Kammer für $\leq$96 h mit UV-Licht bestrahlt.

Mittels LIBS, in Kombination mit multivariater Statistik, ist es gelungen, durch UV-Licht verursachte Veränderungen im Polyimid nachzuweisen. Zusätzlich wurden Veränderungen in der chemischen Zusammensetzung, aufgrund der Entstehung von Korrosionsprodukten auf Reinkupfer, untersucht und gezeigt, dass H_2S korrosiver wirkt als SO_2.

LA-ICP-MS wurde für die qualitative Messung der Gaspermeabilität in Polyimid optimiert. Die Aufnahme von Tiefenprofilen war erfolgreich. Es wurde herausgefunden, dass die Bewitterung mit SO_2 zu einem signifikanten Anstieg der Intensität des Schwefelsignals führt. Die Zunahme war im oberen Bereich des Polyimids am höchsten und nahm zum Substrat hin ab.

Die Bewitterung mit H_2S resultierte insgesamt in einer kaum messbaren Veränderung. Bei zwei der fünf Polyimide führte UV-Bestrahlung vor der Bewitterung mit H_2S zu einem Anstieg des Schwefelsignals in den oberen Lagen des Polymerfilms.
Mit LIBS und LA-ICP-MS ist es erfolgreich gelungen, Polymerdegradation und Diffusion in Polymeren zu messen. Diese Ergebnisse legen nahe, dass SO_2 einfacher in Polyimid eindringt als H_2S und, dass UV-Bestrahlung die Permeabilität signifikant beeinflussen kann und zu messbarer Degradation des Polyimids führt.

Contents

List of Figures

List of Figures

Abbreviations

Ar	argon
Cu	copper
H_2S	hydrogen sulfide
He	helium
NO_2	nitrogen dioxide
O_3	ozone
SO_2	sulphur dioxide
S	sulfur
a.u.	arbitrary units
CCD	charged coupled device
CRM	certified reference material
fs	femtosecond
FTIR	Fourier-Transform Infrared Spectroscopy
ICP	Inductively Coupled Plasma
LA	Laser Ablation
LA-ICP-MS	Laser Ablation Inductively Coupled Plasma Mass Spectrometry
laser	Light Amplification by Stimulated Emission of Radiation
LIBS	Laser Induced Breakdown Spectroscopy
m/z	mass to charge ratio
MFG	mixed flowing gas
MLs	monolayers

MS	Mass Spectrometry
Nd:YAG	neodymium-doped yttrium aluminum garnet; $Nd:Y_3Al_5O_{12}$
NIST	National Institute of Standards and Technologies
NMP	N-Methyl-2-pyrrolidone
ns	nanosecond
PCA	Principal Component Analysis
PI	polyimide
PIs	polyimides
ppb	parts per billion
PTFE	polytetrafluoroethylene
RF	radio-frequency
RH	relative humidity
S/N	signal-to-noise ratio
T	temperature
T_g	glass transition temperature
UV	ultraviolet

1. Introduction

Investigation and understanding of corrosion mechanisms are key to ensure the reliability of many produced goods. This is especially true in the field of microelectronics. Microchips, for example, are designed to have specific properties. Corrosion, however, alters the material and change those properties - sometimes even leading to product failure - and occurs in many different ways. One of these paths, atmospheric corrosion, was investigated more closely in this thesis (Jacobsen et al., 2014; Ambat, Jensen, and Moller, 2008; Valdez Salas et al., 2013a).

According to Leygarf, 2016 global cost estimates for atmospheric corrosion reach values as high as US$ 100 million per year. Over the last decades a lot of research has therefore been conducted in this field and standard practice guides for environmental testing, such as the American Society for Testing and Material (ASTM), 1997, have been developed to give experiments a fixed frame and make results more comparable. Accelerated stress tests are commonly used to investigate the behavior of complex structures under harsh conditions (Osenbach, 1996).

Currently used experimental techniques in the field of atmospheric corrosion are mostly surface sensitive (e.g. FTIR (Fourier-Transform Infrared Spectroscopy) and raman spectroscopy) or based on detecting changes in the mass or electronic properties of the investigated material. While many problems can be solved by using these techniques, in some cases, they are insufficient or too time consuming (Leygarf, 2016).

Problems arise, for instance, when working with microchips. In a simplified manner, the basic set-up of a microchip can be described as follows: a silicon wafer as substrate, followed by a thin metal layer (e.g. copper, aluminum) to connect different electrical components and a protective, insulating layer on top of it. For this purpose polymers (e.g. PI) are often employed. These layers need to withstand harsh environmental conditions such as corrosive gases (e.g. SO_2 (sulphur dioxide) and H_2S (hydrogen sulfide)). To provide

optimal protective properties the polymer should not degrade under these conditions and should prevent alteration of the underlying material. Another advantage is the low dielectric constant that polymers usually have.
However, protecting the metal with a polymer layer takes away the possibility for direct investigation of the metal-polymer and substrate-metal interfaces with surface sensitive methods. Therefore, laser (Light Amplification by Stimulated Emission of Radiation) based techniques present a promising alternative. They are quick measurement techniques and allow depth profiling of the investigated samples, thereby enabling examination of different sample domains without prior preparation. Looking at the protective layer, depth profiling provides information on changes in its chemical composition or transport processes of chemical species within it. After ablation of the protective layer analysis of the underlying metal layer is possible. The feasibility of such corrosion and material alteration measurements using LA-ICP-MS (Laser Ablation Inductively Coupled Plasma Mass Spectrometry) and LIBS (Laser Induced Breakdown Spectroscopy) were investigated in this thesis (Tummala, Rymaszewski, and Klopfenstein, 2012; Ho et al., 1985; Madani, Vedage, and Granata, 1997; Yeh, 1986; Pisonero and Detlef Günther, 2008; Pouli et al., 2005; Grundmeier, Schmidt, and Stratmann, 2000).

A feasibility study was conducted, followed by optimization of the measurement parameters to the required analytical information. Samples of interest (polyimide and copper) were stressed in a humid atmosphere containing corrosive species (SO_2 or H_2S) and later analyzed using the aforementioned laser based methods. For one experiment, samples were additionally subjected to varying UV (ultraviolet) light exposure times prior to the environmental stress tests. Additional measurements were done using optical microscopy.

Aside from the feasibility, one aim was to determine possible alteration of the protective layer due to the UV exposure and weathering. Another was to examine how the S (sulfur) concentration in the polyimide film changed due to the weathering with corrosive species that contain S.

2. Theoretical background

2.1. Corrosion

Corrosion is an electrochemical reduction-oxidation process. For it to occur the following four components must be present:

1. a (metal) anode
2. a (metal) cathode
3. a conductor between anode and cathode
4. an electrolyte (a salt containing solution) in contact with anode and cathode

Anode and cathode can be metals of different nobility or, due to heterogeneities (e.g. lattice defects), two sites of the same metal. As one of the metals/one site is nobler than the other a potential difference is established. The difference in potential can also be caused by differences in concentration of the electrolyte at the anode and cathode. Reduction occurs at the cathode, oxidation at the anode. The oxidation of the metal at the anode leads to positively charged metal ions and free electrons. This process can, among other possible outcomes, result in the dissolution of the metal and consequently in the formation of pits. A possible alternative is the formation of an oxide layer on the surface, which serves to protect the underlying metal from further corrosion. The latter process is sometimes advantageous, but problematic, for instance, when working with microelectronic devices, because it can result in anode/cathode short failures (Schweitzer, 1999; Osenbach, 1996).

2.1.1. Atmospheric corrosion - basics

The following two chapters provide an overview of atmospheric corrosion. For detailed information on atmospheric corrosion refer to Leygarf (2016) and references therein.

Atmospheric corrosion is one of many ways in which corrosion occurs. As such, the elements listed in the previous section (section 2.1) apply. For atmospheric corrosion the electrolyte is supplied by the surrounding atmosphere and is therefore usually water in the form of rain, fog, dew, the melting of snow or (high) humidity. Typically for corrosion only liquid (electrolyte) and solid (electrode) phase and their interface play a role. However, in this case, the gas phase is also of importance. The following paragraphs provide a brief conceptual overview of atmospheric corrosion mechanisms (Schweitzer, 1999).

The initial phase is between the solid and the gas phase. Water molecules in the atmosphere react with the solid and form metal-oxygen or metal-hydroxyl bonds, resulting in a mono-hydroxyl-layer. After this fast process (fractions of seconds) further adsorption of water molecules leads to the (reversible) formation of additional MLs (monolayers) of water, with properties similar to bulk water. The thickness of this liquid layer depends on several factors, e.g. RH (relative humidity), exposure time and the substrate. Empirical tests have shown an average amount of about 8 MLs at 80% RH.

The dominant atmospheric corrosion reactions are:

$$\mathrm{Me} \longrightarrow \mathrm{Me}^{n+} + \mathrm{ne}^- \quad \text{(anode reaction, metal dissolution)}$$

$$\frac{1}{2}\mathrm{O}_2 + \mathrm{H}^+ + 2\,\mathrm{e}^- \longrightarrow \mathrm{OH}^- \quad \text{(cathode reaction, oxygen reduction)}$$

Due to the excessive amount of oxygen in the atmosphere the anodic reaction tends to be rate-limiting rather than the cathodic (Leygarf, 2016).

The liquid layer is not only the environment where reactions take place, it also acts as a solvent for atmospheric constituents (gases/particulate matter). Some of these species have a known influence on atmospheric corrosion (e.g. NO_2 (nitrogen dioxide), SO_2, H_2S, O_3 (ozone)). The likely routes to corrosion for SO_2 and H_2S, respectively, are:

$$\mathrm{H_2S}_{(g)} \longrightarrow \mathrm{H_2S}_{(aq)} \longrightarrow \mathrm{H}^+ + \mathrm{HS}^-$$

$$SO_{2(g)} + OH^{\cdot} \longrightarrow HSO_3^{\cdot} \longrightarrow \text{several steps} \longrightarrow H_2SO_4$$

In the former equation the corrodent is HS^-, in the latter it is derived from the dissociation of H_2SO_4 in water. The deposition rate is generally rather low for atmospheric constituents and depends on a number of factors, such as thickness and chemical makeup (for the liquid layer) or wind speed and the type of wind flow (for the gas phase). Temperature, UV radiation and concentration of the corrosive species also play an important role. The dissolution of the gases in water is followed by a number of (electro-)chemical reactions in the liquid layer and at the interface between solid and liquid phase. As time progresses the number of dissolved metal ions increases, until at some point supersaturation is reached and the positive ions react with counterions to form solid precipitates. Thus, like in classical corrosion, with prolonged exposure times more and more of the corroded material is covered with the precipitates (so-called corrosion products). Both, the dissolution of the corroded material as well as the precipitation of corrosion products can cause product failure (Leygarf, 2016; Valdez Salas et al., 2013b; Aastrup et al., 2000; Zakipour, Tidblad, and Leygraf, 1995).
Although focused at depicting data on atmospheric constituents that are harmful to health, the World Health Organization (WHO) (2000) air quality guideline provides valuable insights on the concentration of gaseous corrosive species, as many of these substances are harmful as well as corrosive. The more recent European Environmental Agency (EEA) (2018) report shows that air pollution has overall decreased since 2000. Still table 2.1 portrays some of the corrosive substances along with their concentrations in the atmosphere (as given in World Health Organization (WHO) (2000)) as benchmarks.

2.1.2. Atmospheric corrosion - laboratory exposures

From table 2.1 it can be seen that over longer periods of time pollutant concentrations in the atmosphere are in the (sub-)ppb (parts per billion) range. Temporary concentrations can be much higher. As corrosion leads to a variety of problems, efforts are undertaken to simulate the involved processes and use the gathered insights to develop countermeasures. The American Society for Testing and Material (ASTM) (2003) published a

Table 2.1.: Corrosive species in the atmosphere and their approximate concentrations, numbers taken from World Health Organization (WHO) (2000); ppm = parts per million

corrosive species	**atmospheric concentration** (24 h mean) (ppm)	**maximum reported atmospheric concentration** (x h mean) (ppm)
O_3	≤ 0.060	0.26 ($x = 1$)
SO_2	< 0.175	n.a.
H_2S	~ 0.0002	12000 ($x = n.a.$)

standard guide and a standard practice for MFG (mixed flowing gas) tests for electrical contacts. The latter provides procedures for MFG tests and the other presents different techniques and test sets to be conducted based on the standard practice. In the standard guide the proposed test sets are summarized in a table, which is depicted here in figure 2.1. From the parameters in figure 2.1 it is clear that:

1. used concentrations are higher than (long-term) values observed in reality.
2. corrosion simulations are becoming increasingly complex, with a greater number of species used in the tests.

The development of standard guides is important to make results comparable. However, as finished products as well as corrosion conditions vary greatly, laboratory tests that are comparable to reality are hard to develop and progress is still continuously made. One of the key problem in corrosion testing is time. In reality corrosion mechanisms occur on a timescale of months or years due to the low concentrations of atmospheric pollutants. In the laboratory, exposures are usually limited to days or weeks. As a quid pro quo concentrations are increased, to be able to observe corrosion effects in a shorter period of time. This, along with reduced complexity of the gas composition, certainly leads to deviations from reality. However, many field exposure measurements have been conducted and a number of these found results that were in good agreement with laboratory exposures (Leygraf, 2016; Johan Tidblad et al., 2017; Samie et al., 2007; Zakipour, Tidblad, and Leygraf, 1997).

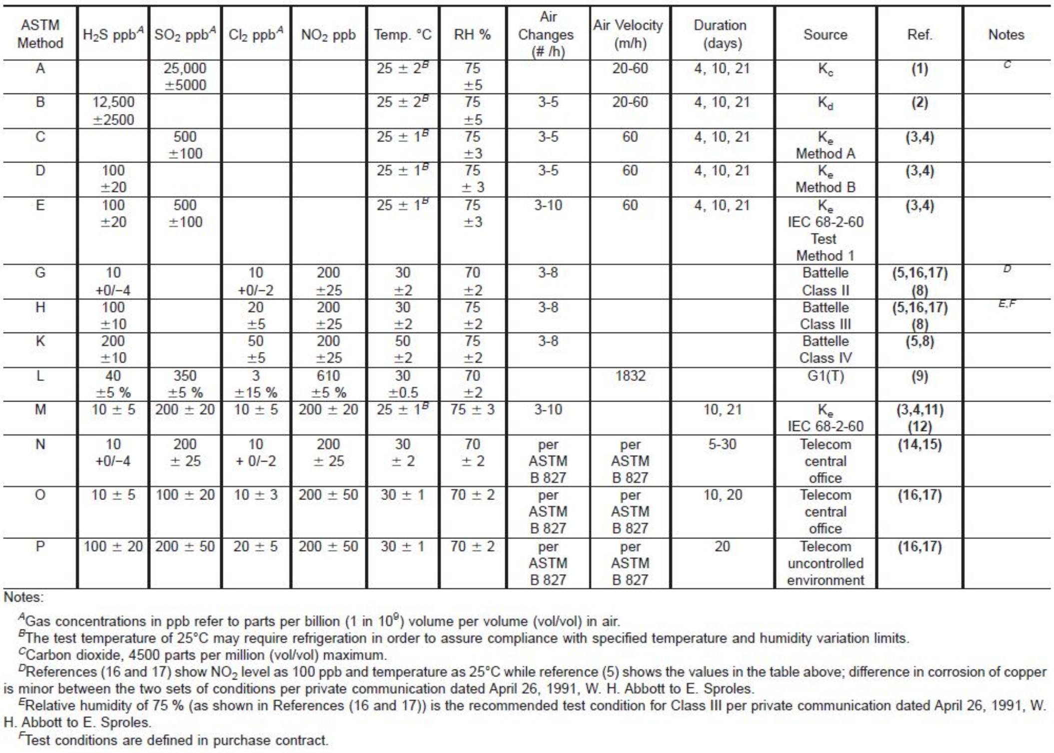

ASTM Method	H_2S ppb[A]	SO_2 ppb[A]	Cl_2 ppb[A]	NO_2 ppb	Temp. °C	RH %	Air Changes (# /h)	Air Velocity (m/h)	Duration (days)	Source	Ref.	Notes
A		25,000 ±5000			25 ± 2[B]	75 ±5		20-60	4, 10, 21	K_c	(1)	[C]
B	12,500 ±2500				25 ± 2[B]	75 ±5	3-5	20-60	4, 10, 21	K_d	(2)	
C		500 ±100			25 ± 1[B]	75 ±3	3-5	60	4, 10, 21	K_e Method A	(3,4)	
D	100 ±20				25 ± 1[B]	75 ± 3	3-5	60	4, 10, 21	K_e Method B	(3,4)	
E	100 ±20	500 ±100			25 ± 1[B]	75 ±3	3-10	60	4, 10, 21	K_e IEC 68-2-60 Test Method 1	(3,4)	
G	10 +0/−4		10 +0/−2	200 ±25	30 ±2	70 ±2	3-8			Battelle Class II	(5,16,17) (8)	[D]
H	100 ±10		20 ±5	200 ±25	30 ±2	75 ±2	3-8			Battelle Class III	(5,16,17) (8)	[E,F]
K	200 ±10		50 ±5	200 ±25	50 ±2	75 ±2	3-8			Battelle Class IV	(5,8)	
L	40 ±5 %	350 ±5 %	3 ±15 %	610 ±5 %	30 ±0.5	70 ±2		1832		G1(T)	(9)	
M	10 ± 5	200 ± 20	10 ± 5	200 ± 20	25 ± 1[B]	75 ± 3	3-10		10, 21	K_e IEC 68-2-60	(3,4,11) (12)	
N	10 +0/−4	200 ± 25	10 + 0/−2	200 ± 25	30 ± 2	70 ± 2	per ASTM B 827	per ASTM B 827	5-30	Telecom central office	(14,15)	
O	10 ± 5	100 ± 20	10 ± 3	200 ± 50	30 ± 1	70 ± 2	per ASTM B 827	per ASTM B 827	10, 20	Telecom central office	(16,17)	
P	100 ± 20	200 ± 50	20 ± 5	200 ± 50	30 ± 1	70 ± 2	per ASTM B 827	per ASTM B 827	20	Telecom uncontrolled environment	(16,17)	

Notes:

[A] Gas concentrations in ppb refer to parts per billion (1 in 10^9) volume per volume (vol/vol) in air.

[B] The test temperature of 25°C may require refrigeration in order to assure compliance with specified temperature and humidity variation limits.

[C] Carbon dioxide, 4500 parts per million (vol/vol) maximum.

[D] References (16 and 17) show NO_2 level as 100 ppb and temperature as 25°C while reference (5) shows the values in the table above; difference in corrosion of copper is minor between the two sets of conditions per private communication dated April 26, 1991, W. H. Abbott to E. Sproles.

[E] Relative humidity of 75 % (as shown in References (16 and 17)) is the recommended test condition for Class III per private communication dated April 26, 1991, W. H. Abbott to E. Sproles.

[F] Test conditions are defined in purchase contract.

Figure 2.1.: test conditions of MFG tests, (American Society for Testing and Material (ASTM), 2003)

2.2. Polyimides

PIs are of great relevance within this thesis. For this reason some important features and information on them are presented in the following.

2.2.1. Polyimide chemistry and properties

PIs are polymers, more precisely they are part of either the class of thermoplastics or thermosets. They are produced by polycondensation or polyaddition. The general chemical structure of PI is depicted in figure 2.2. The polycondensation is based on the reaction of an aromatic diamine with an aromatic dianhydridide. PIs have many handy properties:

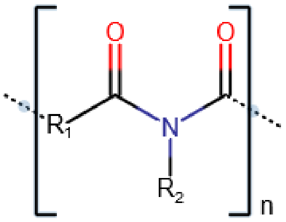

Figure 2.2.: general chemical structure of PI (structure drawn using Chemspace)

- good chemical resistance and insolubility in most solvents,
- high thermal stability, flame- and heat-resistance,
- adhesion, insulation and passivation.

Due to their ability to insulate and passivate at the same time, while also having high thermal stability, PIs are widely used as a protecting layer in the fields of (micro)electronics (DuPont, 2017; Dominighaus et al., 2008; Braun et al., 2012).

2.2.2. Gas diffusion principles with focus on polyimides

As this thesis is focused on investigation of corrosion (resistance) in the context of corrosive gases, the permeability of polyimides deserves extra attention. Of particular interest are SO_2 and H_2S as well as the uptake and permeability of H_2O in the form of moisture. For different films of Kapton® Type FN the moisture absorption at 23 °C ranges from 1.2 % to 2.5 % at 98 % RH, the water vapor permeability lies between 2.4 and 17.5 g $(m^2\,24h)^{-1}$ (DuPont, 2017). Moisture absorption values for PI films seldomly succeed 2 % (Freeman, 2010; DuPont, 2017; Mushtaq et al., 2016).
When looking at the transport properties of species through a polymer one has to differentiate between rubbery and glassy polymers. Rubbery polymer membranes are in operation at temperatures higher than their T_g (glass transition temperature), whereas glassy polymers are not. Sorption in rubbery polymers is analogous to the absorption of gases into a liquid and is thus described by Henry's law,

$$C_{D,i} = k_{D,i} \cdot p_i$$

where $C_{D,i}$ refers to the concentration of the sorbed component i, $k_{D,i}$ is the Henry's law constant, p_i is the pressure in the surrounding gas. The mass transport in this case occurs through sequential jumping from one dissolved sorption site to the next along a chemical potential gradient. In the simplest case the permeability of the rubbery polymer is then described by

$$P_i = D_{D,i} \cdot k_{D,i}$$

with $D_{D,i}$ as diffusion coefficient of the component i through the dissolved mode. In glassy polymers the chains are packed imperfectly and excess free volume is embedded within the polymer matrix. In this free space Langmuir absorption of gases takes place and the solubility is increased. Due to this type of absorption glassy membranes are selective towards gas molecules with a smaller relative size. The kinetic diameters for H_2S, SO_2 and H_2O are 3.6, 3.6 and 2.65 Å, respectively (Freeman, 2010). As Langmuir absorption plays a role in glassy polymers, Henry's law alone is not sufficient to describe the absorption process and another term has to be added:

$$C_i = C_{D,i} + C_{H,i} = k_{D,i} \cdot p_i + \frac{C'_{H,i}}{1 + b_i \cdot p_i}$$

where $C'_{H,i}$ is the Langmuir adsorption capacity of the polymer (i.e. the maximum concentration of absorbed penetrant gas in the polymer) for component i and b_i is the Langmuir affinity of component i for the hole-filling sorption sites. As the number of Langmuir sorption sites, i.e. the free volume, is limited, saturation for this kind of diffusion is obtained at high feed pressures. Based on the given information it is quite comprehensible that processes like annealing reduce gas permeability due to chain relaxation and reduced free volume. Principles of diffusion processes will not be described in any more detail here, but it is important to bear in mind that Langmuir sorption sites are only partially immobilized, ergo still contribute to the total gas diffusion, and that effects, such as polymer plasticization due to the gas (e.g. SO_2 and H_2S), can strongly influence the diffusivity of materials through the polymer. Matsui, Ishiguro, et al. (1997) observed a decrease in permeability of PI membranes due to UV radiation. An exemplary study of SO_2 sorption in a PI is given by Koros et al. (1980) and Felder, Patton, and Koros (1981) (Crank, 1975; Kraftschik, 2013; Freeman, 2010; Yi et al., 2012).

2.3. LASER - Light Amplification by Stimulated Emission of Radiation

For principles of laser operation and certain types of lasers refer to Siegman, 1986, and Orazio, 2010. In this chapter only the Nd:YAG (neodymium-doped yttrium aluminum garnet; $Nd:Y_3Al_5O_{12}$) laser will be described in more detail as it is of relevance for this thesis.

2.3.1. Nd:YAG LASER

A schematic of a Nd:YAG laser is diagrammed in figure 2.3. Nd:YAG lasers belong to the class of solid-state lasers. These have doped ions as an impurity in an otherwise transparent host material. The active material used in this kind of laser is a yttrium aluminum garnet crystal, the doping is done with neodymium (Nd^{3+}). The most popular wavelength emitted by

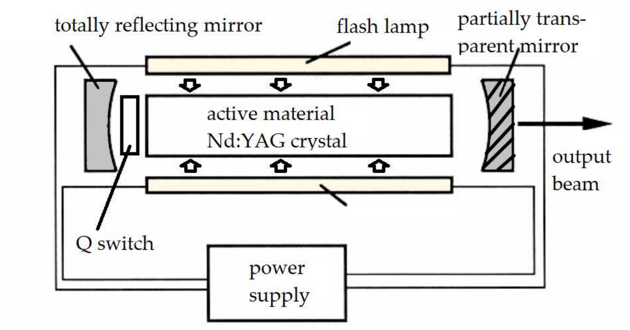

Figure 2.3.: schematic of a Nd:YAG laser

this laser is at 1064 nm(Musazzi and Perini, 2014). Flash lamps pump the light, produce excitation and lead to a “population inversion” in the active material. This in turn results in amplification of the photons passing through the laser rod at the frequency of lasing transition (stimulated emission). The mirrors enhance this effect by reflecting the photons back to the rod. Q switches are introduced into the system as a shutter which opens once maximum population inversion is reached and makes strong laser pulses possible. In science Nd:YAG lasers are often used as Q-switched lasers with their harmonic beams (Musazzi and Perini, 2014; Cremers and Radziemski, 2013; Orazio, 2010).

2.3.2. LASER-matter interaction

A multitude of processes is initiated when a laser pulse is fired at matter. The most important way of transferring energy from radiation to matter is absorption via electrons. Other effects are direct absorption by optical phonons and the stimulated raman effect. This energy input triggers a chain of transformations and leads to an increase in temperature of the material. The heating eventually results in phase transformations, material breakdown, ionization and plasma formation as well as radiation, particle emission and physical modifications of the system (e.g. ablation). For plasma formation to occur a certain threshold laser fluence has to be exceeded. For LIBS plasma formation on solids reported threshold values are in between 10^8 and 10^{10} W cm^{-2} (Cremers and Radziemski, 2013) (Musazzi and Perini, 2014; Cremers and Radziemski, 2013; Orazio, 2010).

In order for a plasma to be formed atoms must be ionized. For gases the principle is as follows:

At least one free electron has to be present to kick off the ionization process. This free electron can, for example, be a transient electron liberated by cosmic rays or originate from multiphoton ionization - that is ionization of an atomic electron caused by simultaneous absorption of n photons with a total energy higher than or equal to the ionization potential of the atom. The free electrons can then ionize further atoms, for instance by cascade ionization. While multiphoton ionization occurs at high irradiances only, cascade ionization has been determined as key mechanism at irradiances encountered in LIBS and LA (Laser Ablation). In cascade ionization a free electron (on average) increases its energy by absorbing energy from the field upon collision with atoms. At some point the energy is sufficient for ionization of an atom and a new electron is generated, which can in turn generate new electrons. That way the cascade process continues (Musazzi and Perini, 2014).

The processes occurring in solid materials are essentially the same as in gases, with the important difference that electronic excitation is quickly passed on to the lattice and transformed into heat via phonon vibrations. An important mechanism in metals (and semiconductors if the energy is sufficient to promote electrons from the valence band to the conducting band) is inverse bremsstrahlung. This describes the absorption of radiation due to electrons in the conducting band through free-free transitions. Upon decay of these excited electrons back to unoccupied lower energy states of the band the freed energy is passed on to the phonons. Heat diffusion properties of the sample therefore play a crucial role. The plasma is generated only after the material is vaporized - at this point, the process continues as described in the above paragraph. If the plasma becomes optically thick it shields the sample surface by absorbing the incoming laser radiation, further heating the plasma (Musazzi and Perini, 2014).

The interaction between laser and matter is strongly dependent on the wavelength and pulse duration. Shorter wavelengths result in a higher ablation efficiency, spatial resolution and reproducibility, better S/N (signal-to-noise ratio) and decreased reflectivity. The latter results in a better energy absorption and energy input. However, lasers with a longer wavelength have a lower threshold fluence. Recent developments have given rise to fs (femtosecond) lasers. The mechanisms explained so far are based on the usage of ns (nanosecond) lasers. When fs lasers are used the pulse duration is too short for interaction between electrons and atoms and also for heat transfer. Therefore multi-photon ionization becomes the major mechanism and the pulse does not directly influence the plasma and heat damage is lower than with ns pulses. Additionally, fs lasers have lower ablation threshold energy values and result in more precise material removal, less fractionation in LA-ICP (Inductively Coupled Plasma)-MS (Mass Spectrometry) and negligible emission from the surrounding atmosphere (Koch and Günther, 2007; Musazzi and Perini, 2014).

2.3.3. Quantification using laser techniques

Accurate and reliable quantification with laser-based techniques poses a number of challenges. For quantification one has to determine the system's response to the analyte at a given concentration and then apply a calibration model for analysis of unknown samples. For successful quantification the measurement parameters should be the same for the standards as well as for the investigated sample. For instrumental parameters this is achieved fairly easily. Still, it is often challenging when laser techniques are applied. Sample (in)homogeneity and morphology have to be considered and especially matrix effects play an important role here and strongly influence the signal obtained per laser pulse. The latter effect originates e.g. from differences in the chemical nature, thermal conductivity or reflectivity of the sample (Cremers and Radziemski, 2013).

Many approaches have been used for quantification with laser techniques. Figure 2.4 summarizes a variety of these for LA-ICP-MS. They can mostly be used in LIBS analysis as well. The simplest way to overcome these obstacles is external calibration using a CRM (certified reference material) with (mostly) matching composition. The availability of these, however, is limited. Another possibility is the fabrication of in-house prepared matrix-matched standards by means of, e.g., pellet preparation (for powders), homogenized tissues (for biological samples) or spin coating (for polymer samples). Correction to an internal standard by use of sample-inherent elements, homogeneous spiking of the sample or application of a thin layer

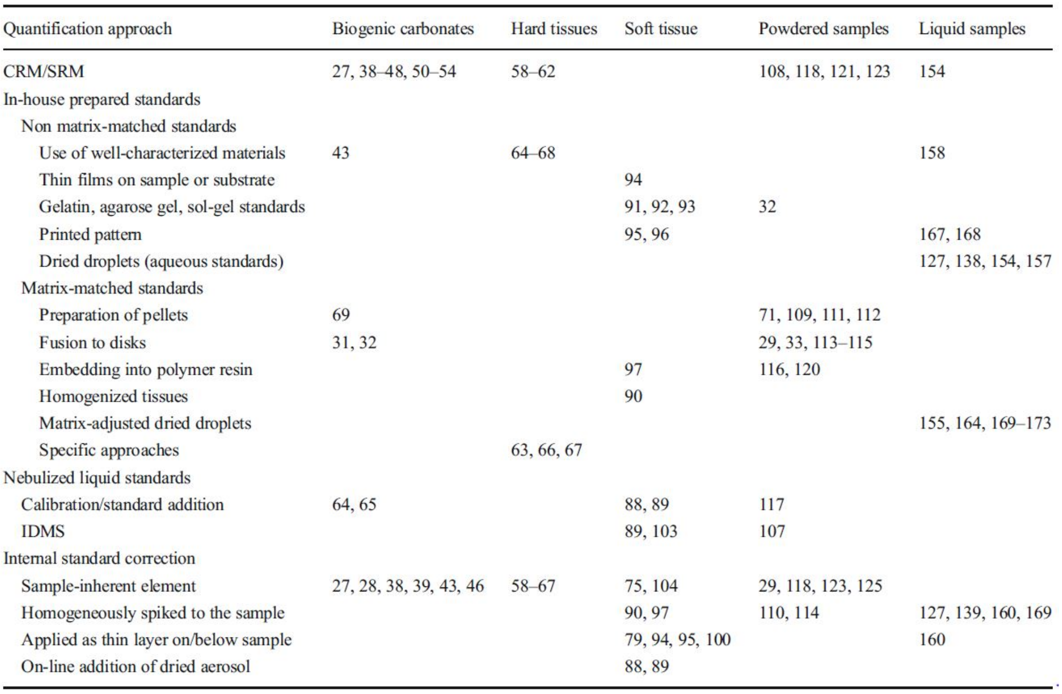

Quantification approach	Biogenic carbonates	Hard tissues	Soft tissue	Powdered samples	Liquid samples
CRM/SRM	27, 38–48, 50–54	58–62		108, 118, 121, 123	154
In-house prepared standards					
Non matrix-matched standards					
Use of well-characterized materials	43	64–68			158
Thin films on sample or substrate			94		
Gelatin, agarose gel, sol-gel standards			91, 92, 93	32	
Printed pattern			95, 96		167, 168
Dried droplets (aqueous standards)					127, 138, 154, 157
Matrix-matched standards					
Preparation of pellets	69			71, 109, 111, 112	
Fusion to disks	31, 32			29, 33, 113–115	
Embedding into polymer resin			97	116, 120	
Homogenized tissues			90		
Matrix-adjusted dried droplets					155, 164, 169–173
Specific approaches		63, 66, 67			
Nebulized liquid standards					
Calibration/standard addition	64, 65		88, 89	117	
IDMS			89, 103	107	
Internal standard correction					
Sample-inherent element	27, 28, 38, 39, 43, 46	58–67	75, 104	29, 118, 123, 125	
Homogeneously spiked to the sample			90, 97	110, 114	127, 139, 160, 169
Applied as thin layer on/below sample			79, 94, 95, 100		160
On-line addition of dried aerosol			88, 89		

Figure 2.4.: selection of procedures for signal quantification in LA-ICP-MS analysis, with permission from Limbeck et al., 2015; numbers in the table are references in the cited paper

on/below the sample has also been reported by several research groups. Another promising procedure, an in-house preparation method with non matrix-matched standards, is the application of dried droplets. This technique can be used as a sort of standard addition by depositing an exact volume of liquid standard on top of a solid sample, evaporating the liquid and ablating the residues of the standard and the solid sample simultaneously. If the amount of ablated standard material is small compared to the amount of ablated solid sample, the matrix is closely related to the matrix of the sample. The obtained signal thus corresponds to the sum of standard and sample signal. For LIBS measurements calibration-free quantification and quantification with assistance of multivariate statistical analysis have also been used. For further information on quantification approaches refer to Limbeck et al. (2015) and Cremers and Radziemski (2013) and references therein (Limbeck et al., 2015; Guenther and Hattendorf, 2005; Musazzi and Perini, 2014).

2.4. LIBS - Laser Induced Breakdown Spectroscopy

LIBS (Laser Induced Breakdown Spectroscopy) is a technique that was first mentioned in the 1960s and has made a lot of progress since then. It is a laser based (atomic) emission spectroscopy that makes use of plasma formation upon impact of a short-pulsed laser on a sample. LIBS has a multitude of advantages that make it an appealing technique:

- Theoretically all elements as well as a number of molecule bands are measurable.
- Full spectra are recorded with each laser shot and analytes of interest can be chosen after the measurement. This also allows not only for univariate but also multivariate data analysis.
- No prior knowledge about the sample and no sample preparation are necessary.
- Mapping and depth profiling of the sample are possible.

The following sections aim to present a brief overview of the basics of LIBS principles, instrumentation and measurements.

2.4.1. Principle and set-up

A standard LIBS-system consists of four main parts (see also figure 2.5):

1. laser source and focusing optics,
2. target container (not obligatory),
3. light collection system,
4. spectral detection system

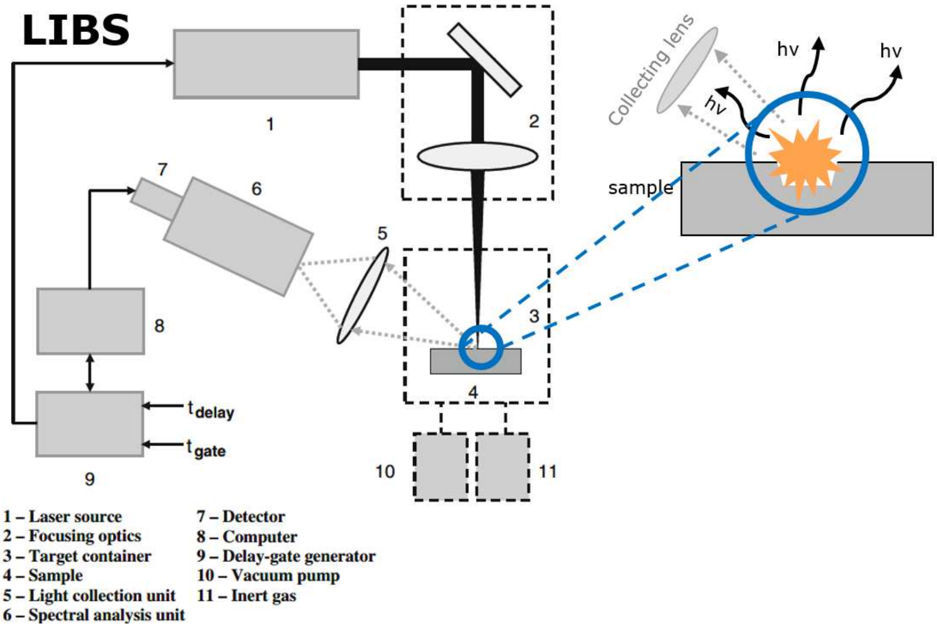

Figure 2.5.: schematic diagram of a LIBS device and the formed plasma caused by a short laser pulse fired on the sample, adapted from Musazzi and Perini, 2014

The first part of the instrument produces the light pulses needed for plasma ignition and directs and focuses them onto the sample. The working principle of a laser is described in chapter 2.3. Typically, for focusing and directing spherical optics are used. In most LIBS devices a laser (or one of its harmonics, see section 2.3.1) is used. The sample is placed in the target container.

In there the interaction between sample and laser pulse takes place. LIBS measurements can be done in a pressurized environment as well as under vacuum, but are mostly conducted under ambient conditions. A target container is therefore not obligatory as long as it is possible to focus the laser pulse on the sample area of interest and the emitted light is successfully collected by the collection system (Skoog, Holler, and Crouch, 2017; Musazzi and Perini, 2014).
The principles of LA and LIBS are closely related. While in LA the ablated material is of interest, in LIBS the light emitted by the formed plasma is investigated. A fraction of the input energy from the laser pulse is transferred to the matter, which in turn leads the formation of the high temperature and high electron-density plasma. More details on laser-matter-interactions are provided in section 2.3.2. For the recording of the emission spectrum it is key to choose an appropriate gate delay - a retention time between laser pulse and recording of the spectrum. After the laser pulse has ended the plasma cools down and excited states decay. Plasma radiation originates from a multitude of transitions as depicted in figure 2.6. As only transitions between certain energy levels are possible, the energy of each emitted photon is characteristic for a specific element. At the start different phenomena such as the stark effect and Bremsstrahlung lead to broad emission lines and a high background signal. These ebb away more rapidly (few hundreds

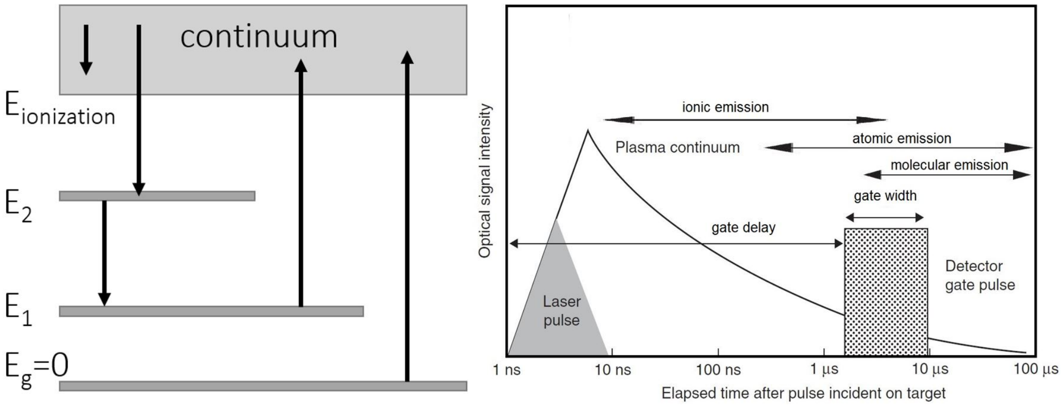

Figure 2.6.: left: schematic diagram of typical transitions in atoms or ions (from left to right: free–free, bound–bound, free–bound, ionization from an excited state, ionization from the ground state); right: schematic overview of the temporal history of a LIBS plasma

of ns) than atomic emission lines and molecule bands (> 10 µs) (Musazzi and Perini, 2014). A gate delay therefore enhances the S/N and results in narrower emission lines. As some emission lines decay more rapidly than others the optimum gate delay depends on the analyte(s) of interest and has to be found in the literature or by empirical studies (Musazzi and Perini, 2014; Cremers and Radziemski, 2013).

In order to analyze the light emitted by the plasma (a fraction of) it first has to be collected and directed to the detector. This can be achieved by using a simple lens and, very commonly in LIBS measurements, optical fibers. The light within the fiber is transmitted by total internal reflection and is guided to the spectral detection system. This system consists of a wavelength-selector unit and an optical detector. The former selects the analyzable wavelength range and at the same time the resolution. For this purpose Czerny-Turner monochromators or echelle polychromators are often employed (Czerny-Turner monochromator: figure 2.7). A Czerny-Turner spectrometer spatially separates polychromatic light into a series of monochromatic rays. The wavelength which is able to pass the exit slit depends on the orientation of the grating. An alternative set-up (in comparison to figure 2.7) would be to use a Paschen-Runge-type spectrometer in which the second mirror directly focuses the diffracted radiation on a multi-element detector instead of maneuvering it through the exit slit.

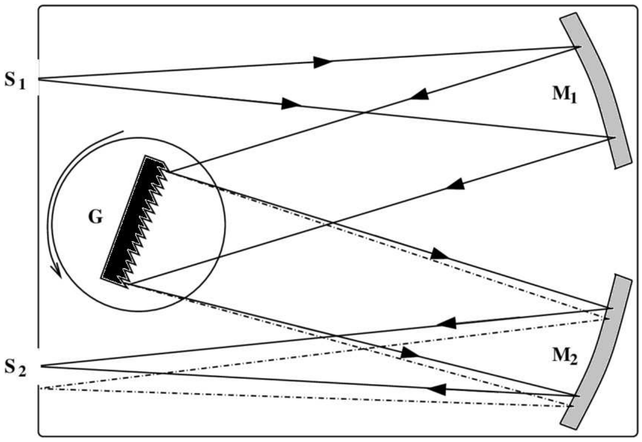

Figure 2.7.: schematic diagram of a Czerny-Turner monochromator, adapted from Pérez León, 2005; (S1 and S2: entrance and exit slits, G: rotatable grating, M1 and M2: spherical mirrors

After the spectrometer the light reaches the detector. The detector has the purpose of converting the optical signal into a recordable and analyzable electric signal. A variety of detectors that find usage in LIBS instruments has been developed. Examples are photomultiplier tubes (see chapter 2.5.1), (intensified) photodiode arrays and (intensified) CCD (charged coupled device). CCD is a plate with light sensitive microscopic areas (pixels) which translate incident photons into electrons. The electrons are collected in charge-packets, amplified, transformed into an output voltage and finally digitally processed (Rivie Krasniker, Valery Bulatov, and Israel Schechter, 2001; Musazzi and Perini, 2014; Cremers and Radziemski, 2013).
With LIBS there are a great many possible applications. All kinds of samples, solid, liquid or gaseous can be investigated and one advantage of LIBS in comparison to other techniques, such as ICP-MS, is the ability to measure light elements (e.g.hydrogen, carbon and oxygen). LIBS instruments have for example been applied for the investigation of geological (e.g. martian rock samples), cultural heritage and biomedical samples (Dyar et al., 2011; Musazzi and Perini, 2014).
Drawbacks of LIBS are for example the difficulty to investigate organic compounds as the molecular information is lost due to atomization of the ablated material or the influence of matrix effects on the measurement, which make quantification difficult (more on the latter is described in chapter 2.3.3). Different approaches have been developed to deal with the loss of molecular information (for an example see section 2.4.3) (R. Krasniker, V. Bulatov, and I. Schechter, 2001; Safi et al., 2018; Musazzi and Perini, 2014).

2.4.2. Sulfur measurements using LIBS

A number of studies have successfully measured S (sulfur) using LIBS. In Dyar et al. (2011) a table of known emission lines for S is given. However, the studies have also shown that S is a weak emitter (due to its high first ionization potential), which results in signals that are much weaker compared to those of other elements. Comparison of barium and sulfur at approximately the same concentration has shown that relative intensities differ by a factor of 100. Due to the sparse irradiation detection limits for S are high compared to most elements and lie in the percent or permille region (Dyar et al., 2011; Gondal et al., 2012).

2.4.3. Polymer measurements using LIBS

As mentioned in section 2.4.1 during LIBS measurements most of the molecular information is lost. This complicates the distinction of materials with a similar chemical structure, as is the case for polymers. However, some molecular bands are retained and observable in the LIBS spectrum and different statistical strategies have been developed and tested for the identification of polymers. While visual examination of the spectrum and univariate analysis might not reveal differences between different classes of polymers, subtle variations are still expected. They originate from varying stoichiometry of the polymer types or differences in laser-matter interactions due to the slightly different matrices. These small differences have successfully been exploited by employing statistical methods, such as ratio determination of different emission lines or molecule bands or PCA (Principal Component Analysis) (Musazzi and Perini, 2014).

2.5. LA-ICP-MS - Laser Ablation Inductively Coupled Plasma Mass Spectrometry

LA (Laser Ablation)-ICP-MS is a form of ICP (Inductively Coupled Plasma) -MS (Mass Spectrometry), which is used to perform measurements directly on solid samples without any sample preparation. It can be used for trace analysis to determine qualitative as well as quantitative elemental composition of unknown samples. Using LA-ICP-MS it is also possible to measure depth profiles.

2.5.1. Principle and set-up

A standard ICP-MS consists of four main parts:

1. sample introduction,

2. ICP and ion focusing optics,
3. mass analyzer,
4. detector.

When using LA-ICP-MS the sample introduction to the ICP-MS is done via LA (figure 2.8). This is achieved by placing the sample in an airtight, closed ablation chamber, the so-called ablation cell, which is flushed with Ar (argon) or He (helium) as carrier gas. By focusing a short (nano-/femtosecond) laser pulse onto the sample surface, material is removed. Through an ablation cup the formed aerosol is flushed into a tubing and transported into the ICP, where ionization takes place (Guenther and Hattendorf, 2005).

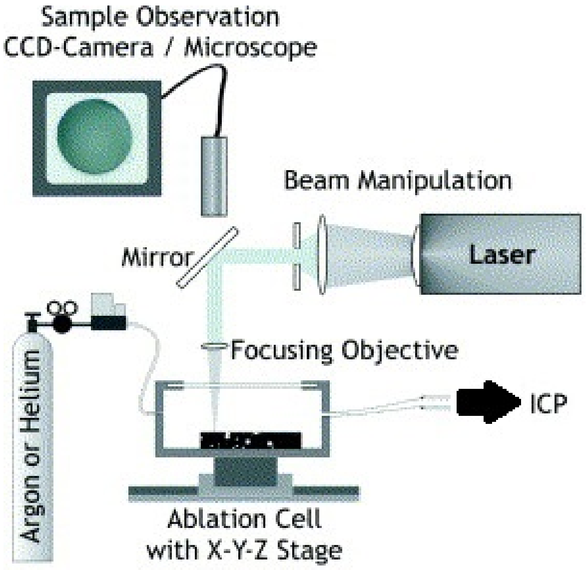

Figure 2.8.: schematic diagram of a LA introduction system, adapted from Guenther and Hattendorf (2005)

A number of parameters influences the ablation, vaporization and ionization efficiency. Many of these parameters are related to the laser: wavelength, repetition rate, pulse duration, pulse energy and diameter. laser-matter interactions are described in more detail in chapter 2.3.2. Other factors that play a role are, apart from general design considerations, carrier gas composition and flow. Typical material removal is at a depth between 0.02 µm and 5 µm per ablated layer. In her review on ICP-MS Beauchemin

(2014) summarizes developments on (LA-)ICP-MS and states, for example, that by using He instead of Ar as carrier gas the particle size is reduced and thus the detection efficiency is increased. Further reading on LA set-up design can also be found therein (Beauchemin, 2014; Guenther and Hattendorf, 2005; Sharp and C. O'Connor, 2007).
Contrary to liquid sample introduction for ICP-MS LA provides a number of benefits:

1. **direct solid sampling**; no sample digestion is needed prior to the measurement, thus resulting in lower sample consumption and reduced contamination.
2. **high sample throughput**; with high repetition rates samples can be analyzed quickly.
3. **quasi non-destructiveness**; laser diameters are as small as 1 µm, making the technique quasi non-destructive (Van Malderen, Elteren, and Vanhaecke, 2015).
4. **spatially resolved analysis**; again due to the variability of the laser diameter, areas of as low as a few microns (as cited in the previous bullet point) can be resolved. This enables the detection of inhomogeneities. While the ability to detect inhomogeneities is in some cases desirable it does at the same time highlight the importance of ablating material over a bigger sample area or at different locations (for bulk analysis) to clarify whether the obtained results are representative for the whole sample.
5. **depth profiling**; due to the material ablation repeatedly focusing the laser on the same spot/area allows for the measurement of depth profiles (see chapter 3.3) (Guenther and Hattendorf, 2005; Sharp and C. O'Connor, 2007).

As mentioned above, the ablated material (for LA-ICP-MS) or the solution of interest (for liquid ICP-MS) is then transported into the plasma torch. The ICP itself is purging a quartz torch with three concentric tubes of different sizes with an inert gas, in most cases Ar (figure 2.9). The Ar is seeded with electrons and those are accelerated in a magnetic field induced by a RF (radio-frequency) energy applied to the induction coil. Upon collision of the electrons with neutral Ar atoms the atoms are ionized. As long as the magnetic field and the gas flow are stable those collisions will continue to happen and the plasma is maintained. The shape of the formed plasma,

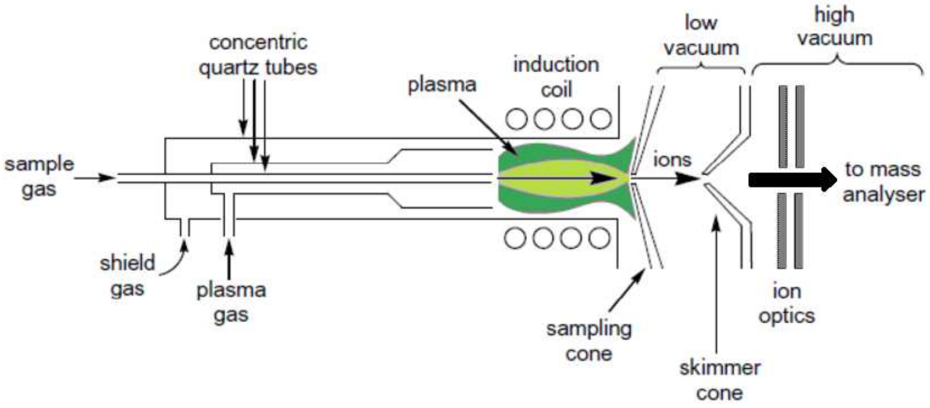

Figure 2.9.: schematic diagram of an ICP and ion sampling interface, adapted from Galazka, 2011

which is determined by the gas flows coming from the outer concentric tubes, is a dense annular-shaped ball. The plasma temperature is between 5000 and 10000 K. In the plasma the introduced aerosol is first vaporized, then atomized, excited and ionized. The ionization process and efficiency depend on the plasma properties and the element. Incomplete dissociation of molecules or re-association of atoms lead to the formation of polyatomic ions, which often have similar masses as the analyte and are therefore detected on the same mass. This effect is called spectral interference (Skoog, Holler, and Crouch, 2017; G. O'Connor and Evans, 2007).

Up to this point, the system is operated under atmospheric pressure conditions. To extract the ions from the plasma and transfer them to the mass analyzer increasing vacuum and a constant electric potential are applied. This is done by using two cones (sampling and skimmer cone) followed by ion-focusing lenses (see figure 2.9). The lenses make use of the fact that ions are (in this case: positively) charged particles and thus manipulated by electrical fields. While the positive ions are focused and accelerated, electrons are repelled (G. O'Connor and Evans, 2007).

In the mass analyzer the extracted ions are separated according to their m/z (mass to charge ratio). At this point, the system operates under vacuum conditions ($< 1.3 \times 10^{-4}$ Pa) (G. O'Connor and Evans, 2007). The mass analyzer is needed for the separation of ions in the ion beam based on their m/z. While there is a number of different mass filters, only the quadrupole

is described in more detail here. Information on the other available devices is given in e.g. Skoog, Holler, and Crouch (2017) (Chapman and Chapman, 1995; G. O'Connor and Evans, 2007).
Figure 2.10 depicts a quadrupole mass analyzer. The set-up consists of four

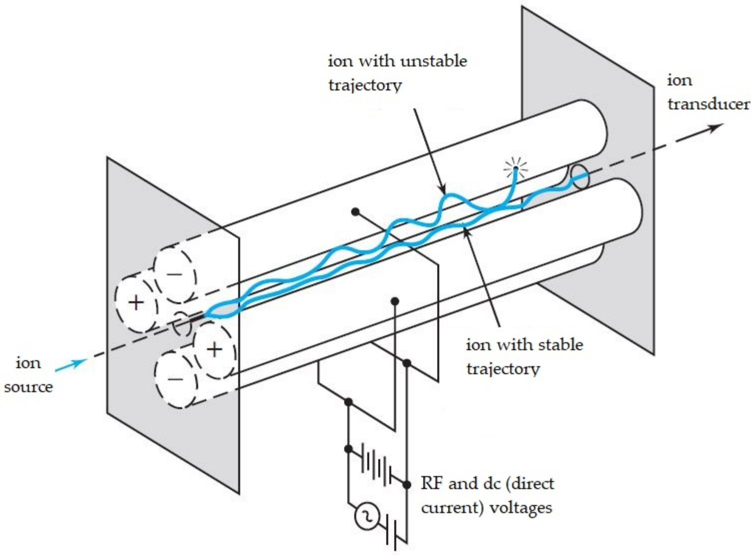

Figure 2.10.: schematic diagram of a quadrupole mass analyzer, adapted from Skoog, Holler, and Crouch, 2017

metallic rods with a variable RF direct current and a variable alternating current applied to them. The rods opposite to one another are in phase, whereas the other two are phase shifted by 180°. Simultaneous alteration of the applied voltages at constant ratio (ac/dc) results in oscillation of the ions passing through the mass analyzer. The oscillation is based on the m/z and only ions of one m/z pass through the filter at any time, the rest collides with the rods and is neutralized (see figure 2.10) (G. O'Connor and Evans, 2007; Chapman and Chapman, 1995).
The quadrupole mass analyzer scans whole m/z ranges in a short period of time (few milliseconds) with the possibility to resolve ions with a mass difference of about one. For ICP-MS measurements this means, that polyatomic interferences with m/z differences in the decimal places can not be distinguished from an analyte of interest (Skoog, Holler, and Crouch, 2017).
The final part of the ICP-MS system is the detector. The purpose of the

detector is to measure the amount of transmitted ions by converting them into electrical pulses and magnifying those. There are a number of devices available for this purpose, the ones of interest for this thesis are the electron multiplier and the faraday cup collector. The latter consists of a collector electrode surrounded by a cage, which prevents detected ions from escaping the detector. Incoming ions from the mass analyzer hit the grounded electrode and are neutralized due to the earthing, leading to a potential drop that is amplified and processed. Faraday cup collectors are commonly used for the measurement of high ion concentrations. An electron multiplier can detect and amplify small currents ($< 10^{-15}$A) and is the most widely used type of detector (G. O'Connor and Evans, 2007). In principle an electron multiplier works in one of two ways: as (a) continuous dynode or (b) discrete dynode electron multiplier. The ions enter the detector and strike either a (a) curved glass tube doped with lead for conductivity or (b) the first dynode in an array of dynodes coated with a metal oxide. These collisions lead to the ejection of secondary electrons which are then accelerated down the curved glass tube by applying voltage or along the series of dynodes by a magnetic field. These electrons again collide along the way, creating a so-called electron avalanche. This process strongly increases the signal, which is then read out at the base of the multiplier (Skoog, Holler, and Crouch, 2017; G. O'Connor and Evans, 2007).

LA-ICP-MS has a broad range of possible applications. Some of these are in the fields of biology, geology and cultural heritage research. For the last field the aforementioned non-destructiveness and direct solid sampling are prerequisites (Vonderheide et al., 2007; Miles and Cook, 2007; Giussani, Monticelli, and Rampazzi, 2009).

As LA-ICP-MS is a laser technique, matrix effects play a great role when it comes to quantitative analysis. Obstacles and possibilities to overcome them are presented in chapter 2.3.3.

2.5.2. Sulfur measurements using LA-ICP-MS

The measurement of S, or light and nonmetallic compounds in general, with LA-ICP-Q-MS (the "Q" signifies that a quadrupole mass analyzer is employed) is rather difficult compared to most metallic compounds. This is due to a number of reasons:

1. Ionization in the Ar plasma is worse than for metals. The 1st ionization potential of S ($S \longrightarrow S^{+} + e^{-}$, 999.6 kJ/mol (≈10.36 eV)) is higher than that of any metal and results in lower ionization efficiency (Huheey, 1997).
2. With typical commercial ion optics the transmission from the ICP to the MS is less efficient for the relatively light sulfur compared to heavier elements.
3. Sulfur has four stable isotopes (see Table 2.2). Of the stable sulfur isotopes ^{32}S is by far the most abundant. The second most common (about $\frac{1}{20}$th) is ^{34}S. On m/z 32 and 34 there is a number of polyatomic interferences that are problematic when trying to measure S. The most common for ^{32}S and ^{34}S, respectively, are:
    - $^{16}O-^{16}O$, $^{14}N-^{18}O$, $^{14}N-^{16}O-^{1}H-^{1}H$
    - $^{16}O-^{18}O$, $^{16}O-^{16}O-^{1}H-^{1}H$, $^{32}S-^{1}H-^{1}H$

    These interferences hinder proper measurements of one or more isotopes. When dealing with possible polyatomic interferences it is also important to look of the relative abundances thereof. In this case, for example, the relative abundances of $^{16}O^{16}O$ is 99.525 compared to 0.200 for $^{16}O^{18}O$. Hence, the latter interference is nearly 500 times less abundant than the former. Consequently, although ^{32}S is ≈20 times more abundant than ^{34}S, measurement of ^{34}S can be advantageous when dealing with a sample that contains oxygen.
4. Existing blank levels for the sulfur isotopes are another limitation for the detection of S. Their existence is ascribed to contaminations due to sulfur in the oil of the ICP-MS, the tubing and seals (Beauchemin, 2014; Laeter et al., 2003; Prohaska, Latkoczy, and Stingeder, 1999; Huheey, 1997).

Table 2.2.: stable isotopes of sulfur and their relative abundances, numbers taken from Prohaska, Latkoczy, and Stingeder (1999)

isotope	^{32}S	^{33}S	^{34}S	^{36}S
relative abundance (%)	94.99	0.75	4.25	0.01

One way to overcome the difficulties caused by spectral interferences is the application of a reaction cell with oxygen as reactive gas as described in the following chapter 2.5.3. Using a reaction cell sulfur can be oxidized to $^{32}S^{16}O$ and thus the m/z interference due to $^{16}O-^{16}O$ is circumvented. Further options are instrumental set-ups with higher mass resolutions, such as double-focusing sector field ICP-MS, or a so-called 'triple quadrupole' MS. The latter, if operated in MS/MS mode, consists of three mass filters. In this case the first quadrupole filters a desired m/z (e.g. ^{32}S) prior to introduction into an ion-guide (quadrupole/octapole), which is filled with a collision/reaction gas, and the final quadrupole again filters the desired m/z (e.g. 48 for analysis of $^{32}S^{16}O$ if oxygen was used as reaction gas) (Prohaska, Latkoczy, and Stingeder, 1999; Bishop et al., 2016).

2.5.3. Collision and reaction cell technology

One of the previously mentioned ways of dealing with polyatomic interferences is the usage of a collision or reaction cell. The collision/reaction cell is located after the ion optics and before the quadrupole mass analyzer. (Figure 2.11). A collision cell is based on the fact that polyatomic species have a bigger collision cross-section than monoatomic ones. Therefore, if the

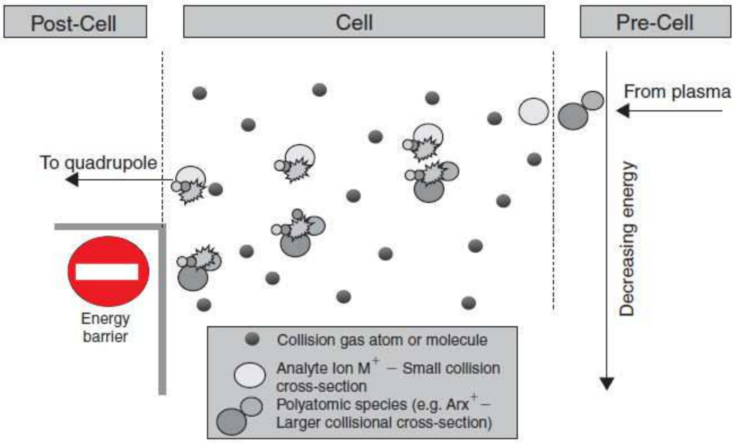

Figure 2.11.: schematic diagram of a collision/reaction cell, adapted from Hill, Fisher, and Foulkes (2007)

collision cell is filled with an inert gas (e.g. helium), the polyatomic species collide with the gas more frequently and lose more kinetic energy upon passing the cell. An applied retarding potential acts as an energy barrier and prevents species with low kinetic energy from entering the mass analyzer. The principle of the reaction cell is similar to the principle of the collision cell. However, in this case the gas that is applied (e.g. oxygen) achieves different outcomes. The reaction gas can, for example, be used to neutralize unwanted polyatomic interferences or, if interfering species are present at the desired m/z, to react with the analyte (e.g. by oxidation) and shift it to a higher, interference-free m/z (Bandura, Baranov, and Tanner, 2001; Hill, Fisher, and Foulkes, 2007).

2.6. TANDEM LA-ICP-MS/LIBS - combining LIBS and LA-ICP-MS

LIBS and LA-ICP-MS are both techniques based on ablating material using a laser. Several research groups have tried to use these two techniques simultaneously - an approach called tandem LA-ICP-MS/LIBS - and thereby combine their benefits. Analysis by these two techniques at the same time is complementary. That way each laser pulse provides an emission as well as a mass spectrum of the same sample spot. LIBS enables measurement of light elements such as hydrogen, carbon and oxygen, LA-ICP-MS has lower detection limits for trace elements and allows detection of different isotopes. The set-up of a tandem LA-ICP-MS/LIBS is a combination of a LIBS instrument with a ICP-MS. In this case the LIBS sample chamber serves at the same time as ablation cell for the LA and is connected with the ICP-MS. One of the challenges going along with tandem LA-ICP-MS/LIBS is the design of the ablation cell. The cell has to allow collection of the emitted light and also have a low washout time in order to preserve rapid measurements. Washout time means the time that is needed to flush all of the aerosol that is formed due to the laser pulse out of the ablation chamber and to the ICP-MS. Apart from the washout, a compromise has to be made regarding optimization of the measurement parameters for LIBS and LA, as optimal settings for two are not (necessarily) congruent (Chirinos et al.,

2014; Bonta and Limbeck, 2018).
Tandem LA-ICP-MS/LIBS has successfully been deployed for, e.g., elemental analysis of coal and archaeological samples as well as metal analysis in polymers. Also 3-dimensional elemental imaging has been done (Chirinos et al., 2014; Bonta and Limbeck, 2018; Dong et al., 2015; Syta et al., 2018).

3. Experimental

In this chapter an overview over the samples, experimental set-up and parameters used in this work is provided.

3.1. Samples and preparation

In the course of this master thesis, six different PIs (polyimides) as well as pure copper wafer samples (without a PI film) were analyzed. Five of the PIs, referred to as PI1 to PI5 within this thesis, were provided by an industrial partner.
Each of the obtained wafers had a silicon substrate with a uniform PI layer with a thickness of about 6 µm on top of it. Also, one additional wafer with a copper substrate protected by a film of PI1 was received. Pure copper samples were also provided. For the experiments wafer pieces of approximately 10 mm x 20 mm were cut from the round wafers with a diamond cutter.
The sixth PI that was used, named P84, was obtained in the form of a commercially available powder, which is soluble in NMP (N-Methyl-2-pyrrolidone).

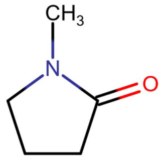

Figure 3.1.: chemical structure of N-Methyl-2-pyrrolidone (structure drawn using Chemspace)

Solutions of about 20 wt% P84 in NMP were prepared and then used for spin coating on 10 mm x 10 mm silicon wafer pieces.

3.1.1. Spin coating

For spin coating a KLM Spin-Coater SCV by Schaefer-Tec AG was used. Parameters for the spinning and tempering process were chosen in order to obtain a desired thickness for the used polymer solution. The corresponding spin coating process is schematically depicted in figure 3.2. The spin coating resulted in PI films with a thickness of about 9 µm.

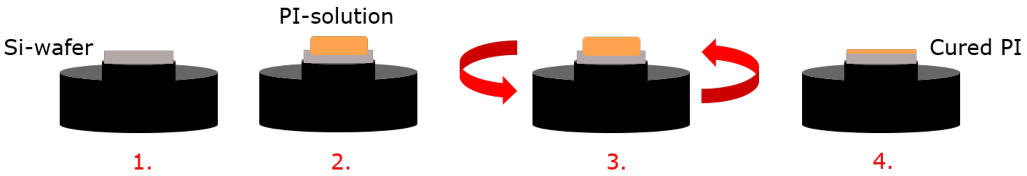

Figure 3.2.: schematic of the spin coating process

3.1.2. UV exposure and weathering with corrosive gases

Throughout this thesis the term “**weathering**” will be used in context of sample exposure to a corrosive atmosphere, i.e. corrosive gaseous species and RH. The term “**alteration**” will be used to refer to UV exposure and its effects.

First preliminary weathering and alteration experiments were conducted with the in-house produced PI samples using polyimide P84. Two samples were altered in a UV chamber (table A.1) for 168 h and two other samples were weathered for 168 h in an atmosphere containing 50 ppm H_2S. Three major weathering and alteration experiments were conducted within this thesis. Two of these consisted of weathering in an atmosphere with corrosive gases only (1st: SO_2, 2nd: H_2S), the third one included a UV-degradation step prior to the weathering. Each of the weathering experiments was conducted in a humid atmosphere. The air (“Luft 5.0”) and gases were obtained from

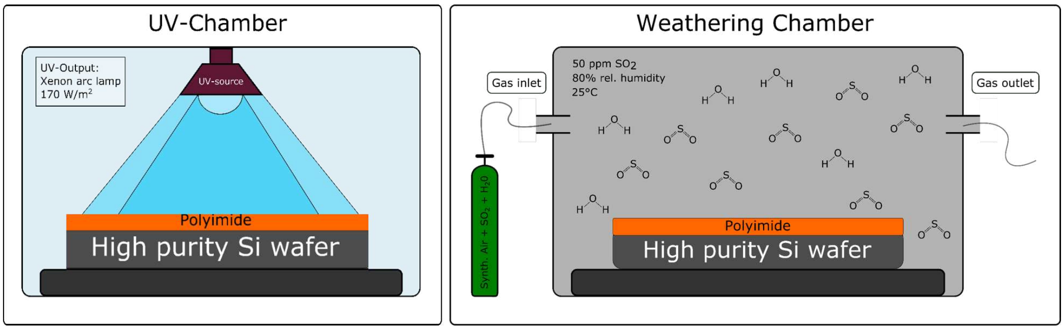

Figure 3.3.: schematic of the UV (left) and weathering chamber (right)

Messer Austria GmbH. The RH was modulated by driving the compressed air through double-distilled water. For these experiments facilities at the Academy of Fine Arts Vienna were used. Schematics of the UV-chamber as well as the weathering chamber (built in-house) are depicted in figure 3.3. The UV-meter basic by Dr. Hönle AG UV-Technology (Munich, Germany) was used for measurement of the UV irradiance. More detailed insights on the gas mixing set-up can be gained from figure A.1 in the appendix. The used parameters were chosen based on prior literature research and are summarized in table 3.1.

Table 3.1.: used parameters for the conducted LIBS measurements

series	A	B	C
corrosive gas	SO_2	H_2S	H_2S
corrosive gas concentration (ppm)	50	50	50
weathering duration (h)	≤192	≤192	≤192
gas flow (L/h)	80	80	80
RH (%)	80±1	80±1	80±1
chamber volume (dm^3)	30.56	30.56	30.56
UV radiation (y/n)	no	no	yes
UV irradiance (W/m^2)			170
UV duration (h)			≤96
T (°C)	22	22	22

3.2. LIBS

For LIBS analysis of the weathered and UV exposed samples a J200 Tandem LA-LIBS instrument from Applied Spectra, Inc. (Fremont, CA, USA), was used. This system is equipped with a 266 nm Nd:YAG laser which is utilized for the ablation of sample material. The optical system consists of a light collecting system with six glass wire channels and a Czerny-Turner spectrometer with a CCD camera. The instrument is shown in figure 3.4. For data acquisition the integrated Aurora software (version 2.0) provided by Applied Spectra along with the instrument, was used.

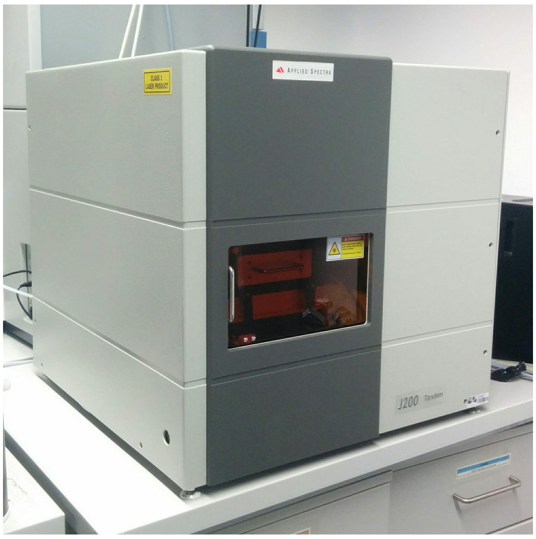

Figure 3.4.: Applied Spectra J200 Tandem; LIBS instrumentation for performed experiments

The measurement parameters were optimized once for the polyimide samples and once for the copper samples, in order to obtain maximum signal to noise ratio for relevant parts of the emisson spectra. 2-D line patterns, with a total number of at least 100 shots, were fired multiple times in the same position to generate depth profiles. Each of the spots gives an emission spectrum. For LIBS spectra presented in this thesis, the intensities acquired from the spot patterns were accumulated (per layer) to make the results more statistically reliable and less prone to errors due to inhomogeneities. For calculation of PCAs the single spectra (each shot) were used. Measurement parameters are pooled in table 3.2

Table 3.2.: used parameters for the conducted LIBS measurements

matrix	laser energy (%)	gate delay (µs)	fluence (J/cm^2)	repetition rate (Hz)	stage velocity (mm/s)	spot diameter (µm)	element: gas flow (L/min)
Cu	50	0.3	29.8	10	0.8	80	Ar: 0.6
PI	60	0.2	22.9	10	1	100	Ar: 1

For data evaluation two softwares were used: the Aurora software and the ImageLab software (version 2.93) by Epina Softwareentwicklungs- und Vertriebs-GmbH (Retz, Austria).
To ensure proper functionality of the whole system, a reference material, the NIST 612 trace metals in glass standard by the NIST (National Institute of Standards and Technologies) was used. If the system was stable and the obtained values at the right order of magnitude, the measurements were directly started. Else, the system had to be tuned first.

3.3. LA-ICP-MS

For analysis with ICP-MS an iCAP Q instrument provided by ThermoFisherScientific (Vienna, Austria; figure 3.5) was used. For the measurements in LA mode the ICP-MS system was connected with the LA system (figure 3.6). The connection between these two was achieved via a PTFE (polytetrafluoroethylene) tubing. The used LA system NWR 213 by New Wave Research, Inc. (Fremont, CA, USA), has a built-in 213 nm (frequency quintupled) Nd:YAG laser. The ablation cell used in this work was made out of aluminum, to avoid possible sulfur contamination due to the use of plastic. During the LA an ablation cup was positioned directly over the ablated region, thus ensuring a rapid and constant washout of the ablated material. For all laser measurements dry plasma conditions were applied.
All LA-ICP-MS results obtained within this thesis were, unless stated otherwise, measured in a measurement mode that has been optimized for

Figure 3.5.: ThermoFisher Scientific iCAP Q; ICP-MS instrumentation for performed experiments

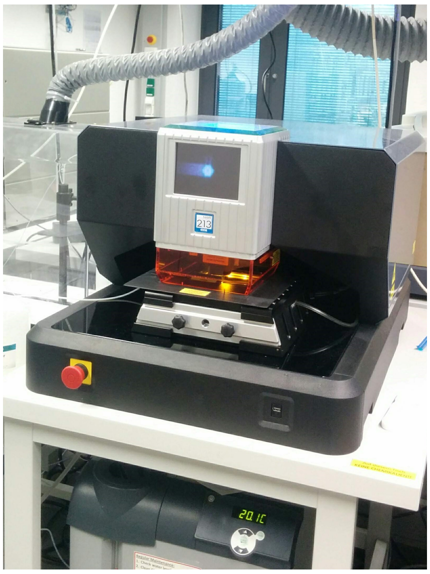

Figure 3.6.: NWR 213 LA system; LA instrumentation for performed experiments

Table 3.3.: used plasma settings for the conducted LA-ICP-MS measurements

auxiliary gas flow (L/min)	coolant gas flow (L/min)	plasma power (W)	measured isotopes	dwell time per isotope (ms)	cone system	measurement mode
0.97	14.0	1400	^{13}C, ^{29}Si, ^{34}S, ^{48}Ti	10	Ni	standard, no collision gas

optimum plasma conditions for LA measurements (table 3.3). The parameters of the laser were optimized for maximum ^{34}S signal while keeping adequate depth resolution. Lines, as shown in 3.7, were fired multiple times in the same position to generate depth profiles. For each layer the averaged background signal was first subtracted from the transient signal. Then the obtained peak signal was averaged, excluding the fringes. For statistical reasons each depth profile measurement was conducted thrice. Ergo, unless stated otherwise, three multiply repeated line scans were measured and the results averaged (for each layer). Consequently, the resulting data points are the average of an average. Measurement parameters are pooled in table 3.4. For data acquisition Qtegra software (version 2.10.3324.62), which was provided with the instrument, was used.

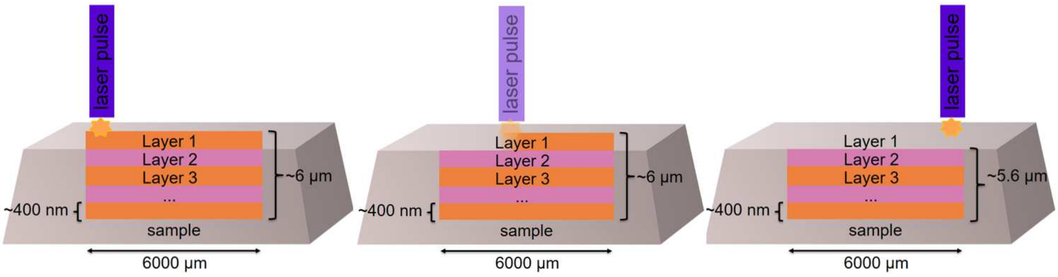

Figure 3.7.: line pattern used for depth profiling with LA-ICP-MS; by constantly firing at the sample while moving the stage a line is ablated (left: first laser pulse, center: half-way through the ablation of the line, right: after ablation of the first line), this process is repeated several times to obtain a depth profile

For data evaluation Microsoft Excel (version 16.0.11629:20246) and a self-

Table 3.4.: used parameters for the conducted LA-ICP-MS measurements

laser energy (%)	**laser fluence** (J/cm^2)	**repetition rate** (Hz)	**stage velocity** (mm/s)	**spot diameter** (µm)	**element: gas flow** (L/min)	**line length** (mm)
50	1.25 - 1.42	20	1	200	He: 0.8	6

written Python program were used. Like for the LIBS system, to ensure proper functionality of the whole system, the NIST 612 trace metals in glass standard by the NIST, was used as reference material and the system was optimized to ^{115}In.

3.4. Profilometry

For profilometric measurements a DektakXT® stylus profiler instrument by BRUKER was used. Data acquisition and evaluation were done using the software Vision64 (version 5.51 update 2) which is provided with the instrument.

Profilometry was used to analyze the depth of the craters obtained from the LIBS or LA-ICP-MS measurements. For this, either single lines or whole maps were scanned. The chosen resolution was 0.367 µm per point and, for map scans, the distance between two measured lines was 30 µm.

4. Results and discussion

In this chapter, the results obtained from the performed measurements are presented and discussed thoroughly. For better clarity they are separated based on the used measurement technique.
When the terms "**H_2S sample**" or "**SO_2 sample**" are used, the author refers to samples that were weathered with H_2S or SO_2, respectively.

4.1. LIBS

The primary aim of the LIBS evaluation was to test the feasibility of this method for the measurement of changes in composition, i.e. corrosion products, polyimide degradation and distribution of chemical species in weathered polyimide. As the samples were exposed to SO_2 and H_2S enriched atmospheres in the weathering experiments, special attention was directed on the element sulfur. Many emission lines of S are known from literature (see chapter 2.4.2), their relative intensities and thus their relevance for actual measurements, however, are harder to determine. For this reason a piece of pure S, sampled at mount Ijen in Indonesia, was recorded with LIBS. The resulting spectrum is depicted in figure 4.1 (intensities are given in a.u. (arbitrary units)). Some of the lines are present due to the surrounding Ar atmosphere and a few lines in this spectrum were attributed to contaminants. The rest of the emission lines that were found in this spectrum, along with the emission lines extracted from literature data were used as library to determine (the existence of) S emission lines in the measured samples.

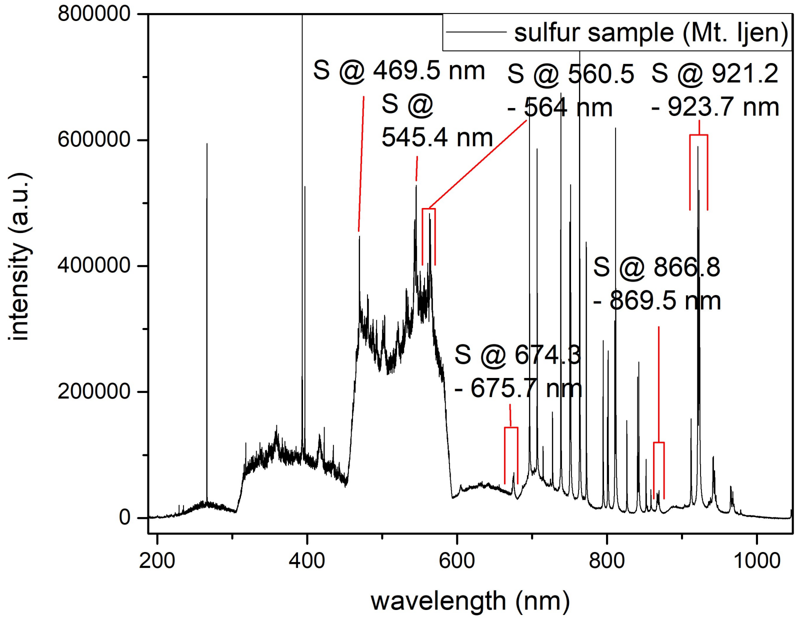

Figure 4.1.: LIBS spectrum obtained from volcanic S, sampled near mount Ijen, East Java, Indonesia, kindly provided by Mag. pharm. Stephan Floriani

4.1.1. Polyimide samples

In total six PIs, PI1 to PI5 as well as the in-house processed P84 were investigated. In a first step, measurement parameters were optimized to achieve maximum S/N on the condition that the energy input is low enough to do depth profiling, i.e. low enough to be able to ablate numerous layers (≥ 5) before reaching the silicon substrate of the wafers. This was achieved by performing measurements with step-wise variation of the parameters and subsequent empirical and numerical evaluation of the spectral areas of interest. The final set of measurement parameters is given in table 3.2. These measurement parameters were used for the recording of the following measurements. One ablated PI layer in LIBS measurements equals ≈1200 nm (for more information see chapter 4.3).

In figure 4.2 an exemplary PI spectrum is presented. The spectrum shows a number of emission lines and molecule bands that have previously been employed for the discrimination of different types of polymers. Prior analyses of polymers with LIBS are described in chapter 2.4.3 and references

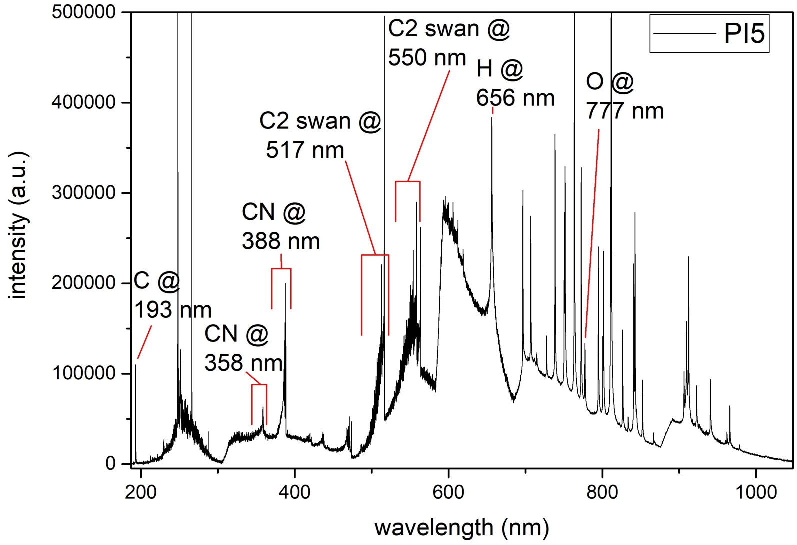

Figure 4.2.: full LIBS spectrum of PI5; emission lines and molecule bands that are commonly observed in polymers are pointed out in red

therein. Molecular bands highlighted in figure 4.2 are the CN-bands around 358 nm and 388 nm and the C_2 swan band, originating from the carbon dimer at 517 nm and 550 nm. Emission lines of interest are C at 193 nm, alpha-hydrogen at 656 nm and the O I triplet at 777 nm. For calculation of PCA other lines were included as well (see table A.2), but these lines and bands were the basis for univariate analysis of the PI samples. Unless explicitly stated differently, all PCAs were calculated with the spectral descriptors given in table A.2 and normalized to the intensity of the CN band at 388 nm. As mentioned in chapter 3.1.2, in addition to three major weathering and alteration experiments a number of preliminary experiments were conducted using the commercial in-house processed PI P84. The results obtained from these experiments are presented in the following and gave direction for the rest of the experiments.

Figure 4.3 shows the spectrum of the first ablated layer, ergo the surface layer, of an untreated sample and another sample that was in the weathering chamber for 48 h in an atmosphere with 50 ppm SO_2. As was stated already in chapter 3.1.2, the RH for this experiment, as for all other weathering experiments, was set to 80 %. It is often hard to distinguish between samples based solely on obvious differences in the LIBS spectra. The characteristic PI

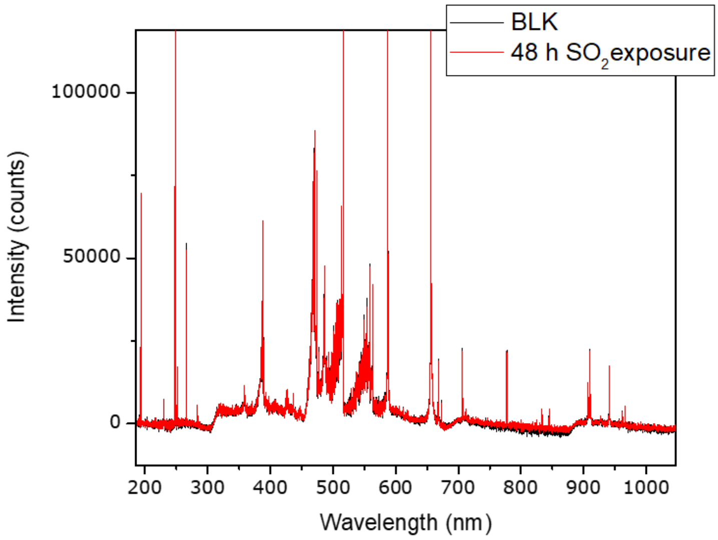

Figure 4.3.: comparison of LIBS spectra of P84, 1st layer of the blank sample and weathered sample (48 h in SO_2 enriched atmosphere)

lines and bands presented previously are, as is to be expected, observable for both samples. No S emission lines were found, neither in the blank nor in the weathered sample. Thus, to determine notable differences between the treated and untreated sample a PCA was calculated. A short description of how to "read" a PCA is given in the following paragraph.

Each point in the PCA is derived from one measurement point, i.e. in this case, one spectrum. Assume that one is dealing with two samples "A" and "B". If these two samples were significantly different from one another, the PCA should reveal these disparities by yielding two different clusters. One should be made up of all spectra from sample "A" and the other of the spectra from sample "B". If this is the case it can reasonably be stated, without knowing the exact cause, that the samples are significantly different from one another.

The PCA calculated from the LIBS spectra as shown in figure 4.3 is given in figure 4.4. A look at the results from the calculation clearly shows that no clustering, as described in the previous paragraph, is recognizable. It is thus concluded that the weathering under the given conditions did not result

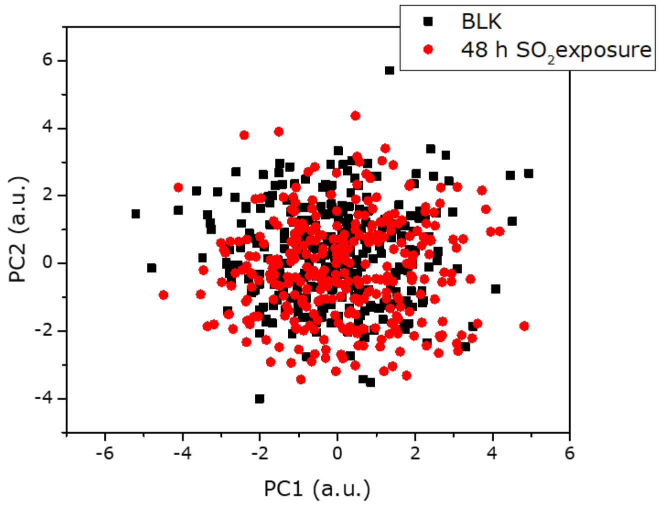

Figure 4.4.: score plot of a PCA of P84, 1st layer of the blank sample and weathered sample (48 h in SO_2 enriched atmosphere), PCA data derived from LIBS data (figure 4.3)

in a detectable change of the PI. Based solely on this measurement, three conclusions are possible. Either measuring polymer degradation with LIBS is not possible, the weathering conditions were not severe or long enough, or the SO_2 does not cause changes in chemical composition and bondings in the polymer. The latter of the conclusions can be argued doubly. Either the barrier properties of the PI are so good that no SO_2 reacts and permeates at all, or SO_2 penetrates and diffuses into the polymer layer but does not react with the PI. This would explain why no changes are observable in the LIBS spectrum. As a consequence of this preliminary measurement it was decided to increase the maximum weathering duration for the weathering experiments to the 192 h given in chapter 3.1.2.

To further pursue the feasibility of measuring polymer degradation with LIBS, two UV aged samples were investigated. As before, a PCA was calculated from the measured LIBS data (see figure 4.5). In this figure two graphs are presented, the left one showing the PCA calculated for the first ablated layer. The one on the right portrays the results obtained for the fifth layer. Unlike in the prior PCA, this time there is a clustering. In the first

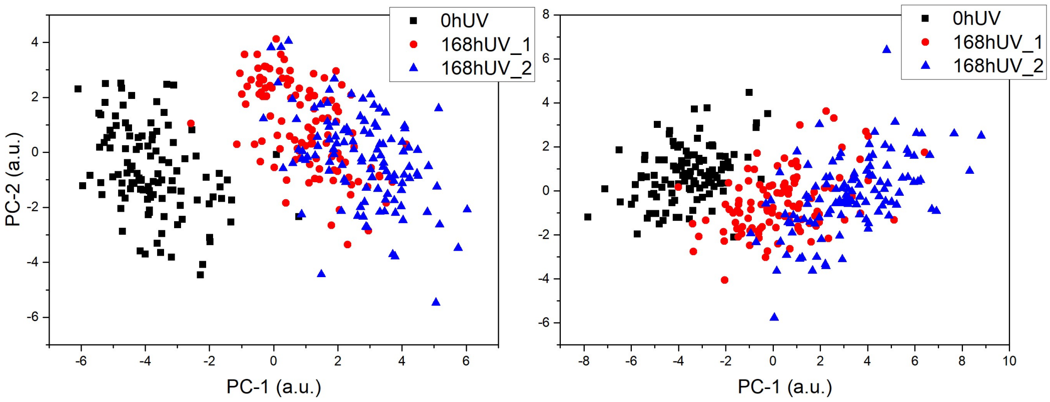

Figure 4.5.: score plot of a PCA of P84, (left: 1st layer of the blank (black) and exposed to UV for 168 h (red and blue); right: 5st layer of the same samples), PCA data derived from LIBS data

layer the UV altered samples are not distinguishable from one another, but clearly from the blank. The fifth layer was the last layer before the silicon substrate was reached. Looking at the graph on the right in figure 4.5 it can be seen that at this point the UV samples are less clearly discernible from the blank, but even this layer still seems to be affected by the treatment. This indicates that, while 192 h are deemed proper for weathering, 168 h in the UV chamber are already too long, as the whole sample is altered. For this reason, a maximum of 96 h UV exposure was chosen for further alteration experiments. This preliminary experiment showed that it is possible to determine PI aging, thus negating the first option stated after the previously discussed weathering experiment. Up to this point it could, however, not be established whether SO_2 permeates the PI or not.

The next and final preliminary experiment was conducted with P84 in an atmosphere containing 50 ppm H_2S for 192 h. H_2S is generally known as the more potent corroding agent when compared to SO_2. In general degradation effects are therefore expected to be more severe with this gas. This, in combination with the increased weathering duration, made the detection of polymer degradation more likely than for the experiment with SO_2. In figure 4.6 the results from the PCA are given. Although more severe conditions were chosen, no polymer degradation was observed. It is therefore assumed, that the PI composition is not significantly affected by weathering with SO_2 and H_2S, at least in the case of this PI.

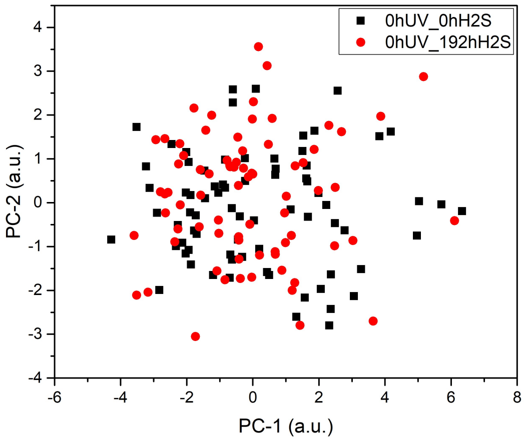

Figure 4.6.: score plot of a PCA of P84 (1^{st} layer), blank and exposed to H_2S (50 ppm) for 192 h, PCA data derived from LIBS data

From the preliminary measurements the following conclusions were drawn:

- The determination of changes in the PI structure is possible. This was successfully shown for a UV altered sample. However, 168 h of UV exposure proved too much to fulfill the requirements of the sample investigation.
- Weathering does not affect the chemical composition of the polymer - at least when samples are used that were weathered for 168 h in SO_2 or H_2S. The interaction between PI and gas can not be measured with LIBS. Thus it is not possible to determine whether the corrosive gas diffuses into the polymer or the polyimide successfully blocks all of the gas.
- S measurements in PI are not possible with the LIBS-system at the given concentrations.

With the knowledge gained from the preliminary experiments the samples from the three main weathering experiments were analyzed.
The preliminary experiments had shown that it is possible to detect chemical changes in the P84 due to UV exposure but also that it is not possible to do the same after weathering. This was tested for the other PIs as well. In the section on LA-ICP-MS results (chapter 4.2) it is demonstrated that two of the examined PIs, namely PI2 and PI5, show the strongest response to UV

exposure followed by weathering with H_2S. Therefore these were subject to critical scrutiny. PCAs calculated from the spectral data of PI5 are given in figure 4.7. It came as no surprise that in the right graph no differences between the treated and untreated (weathered) sample were observed. However, as for P84 168 h of UV exposure were enough to alter not only the topmost layer of the PI but the whole polymer film, it was unexpected that in the case of PI5 not even for the first layer a change was measured - neither for the UV exposure nor UV in combination with weathering. One explanation for this is the reduction of UV exposure time by 50 %, which aimed to make sure that not the whole film was altered. It is also likely that the polymer provided by the company as well as its manufacturing process have been optimized thoroughly to obtain reproducible and high quality results. On the other hand the in-house processed P84 is known not to have the best physical and chemical properties among polyimides and the in-house preparation is certainly less elaborate.

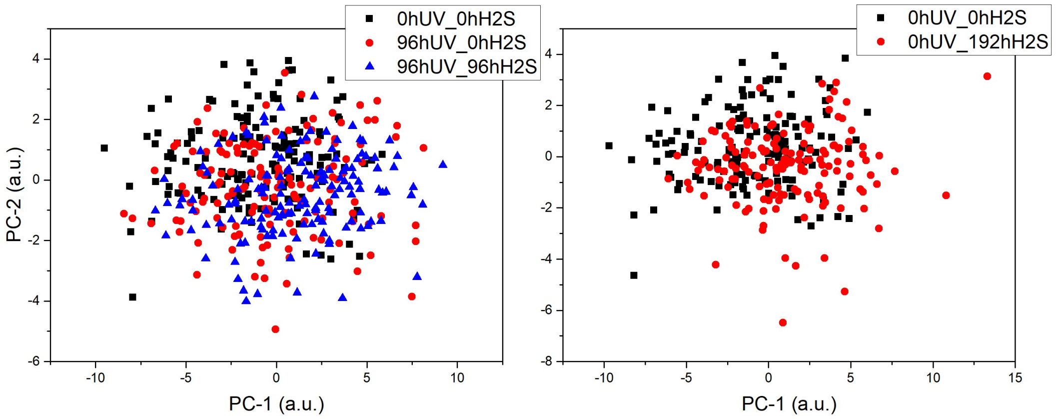

Figure 4.7.: score plots of PCA of PI5 (left: blank (black), exposed to only UV for 96 h (red) and exposed to UV prior to 96 h in H_2S; right: blank (black) and exposed to H_2S for 192 h, PCA data derived from LIBS data

In addition to PI5, selected samples of PI1 were measured. Once again a PCA was calculated from the obtained data and plotted in figure 4.8. In this figure a blank sample (black squares) and a sample that was exposed to UV prior to H_2S weathering (red circles) is portrayed. In the left graph the 1st ablated layer is presented, in the right one the 2nd. This time the result is more similar to the observation that was made for P84. The UV

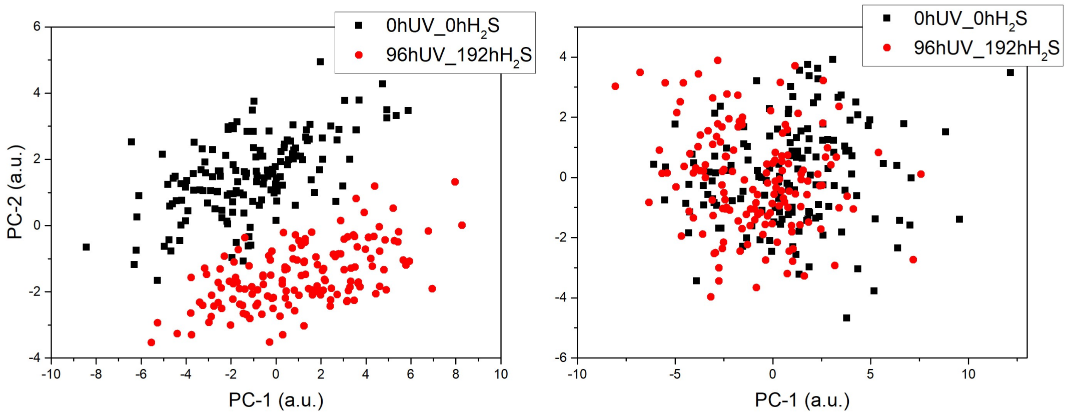

Figure 4.8.: score plots of PCA of PI2 (left: 1st layer of blank (black) and exposed to 96 h UV prior to 192 h in H_2S; right: 2nd layer of blank (black) and exposed to 96 h UV prior to 192 h in H_2S), PCA data derived from LIBS data

exposed sample is distinguishable from the untreated sample, but only in the uppermost layer. Already in the second layer this is not possible anymore. This result confirms that alteration due to UV exposure is possible, as was predicted from the preliminary experiments. Additionally, it shows that PI2 is most susceptible to UV degradation, which will also be discussed in context of LA-ICP-MS measurements (chapter 4.2). Even though, also PI2 was only affected in the first ablated layer at the chosen UV exposure time. As alteration from UV exposure was successfully measured, but only for one of the five industrial PIs, a more extensive study on this topic with increased exposure times (at least the initially chosen 168 h) should be conducted. This was not possible within the scope of this thesis. Also other parameters that lead to polymer degradation (e.g. O_3) are worth being investigated.

4.1.2. Copper samples

In addition to the investigated PI samples, Cu (copper) samples with a weathering duration of a maximum of 24 h were measured. All presented LIBS data in this chapter originates from the first ablated layer of the investigated samples. One ablated Cu layer in LIBS measurements equals $\approx$ 800 nm (for more information see chapter 4.3). Bare Cu is a lot more susceptible to alteration in a corrosive environment than PI. Therefore, though the weathering duration was reduced, expected effects are a lot more significant than those observed in the polymers. This was soon confirmed by visual inspection as alteration of the material, for both H_2S and SO_2, could already be seen after only a few hours in the weathering chamber. In this case LIBS proved to be a simple, yet potent, tool for the weathering effects. Figure 4.9 compares the blank and a Cu sample weathered for 24 h. It shows emission lines that are expected to change due to the formation of corrosion products (e.g. oxides, hydroxides and sulfides) with increasing weathering duration. In this case multivariate analysis is not necessary as the changes are already clearly visible in the spectrum. Moreover, unlike for the PI, the formation of S was also observable in the spectra. In part, the differences in the matrix explain this, but the most likely explanation is that S concentrations on the Cu surface are a lot higher than those in the PIs. It

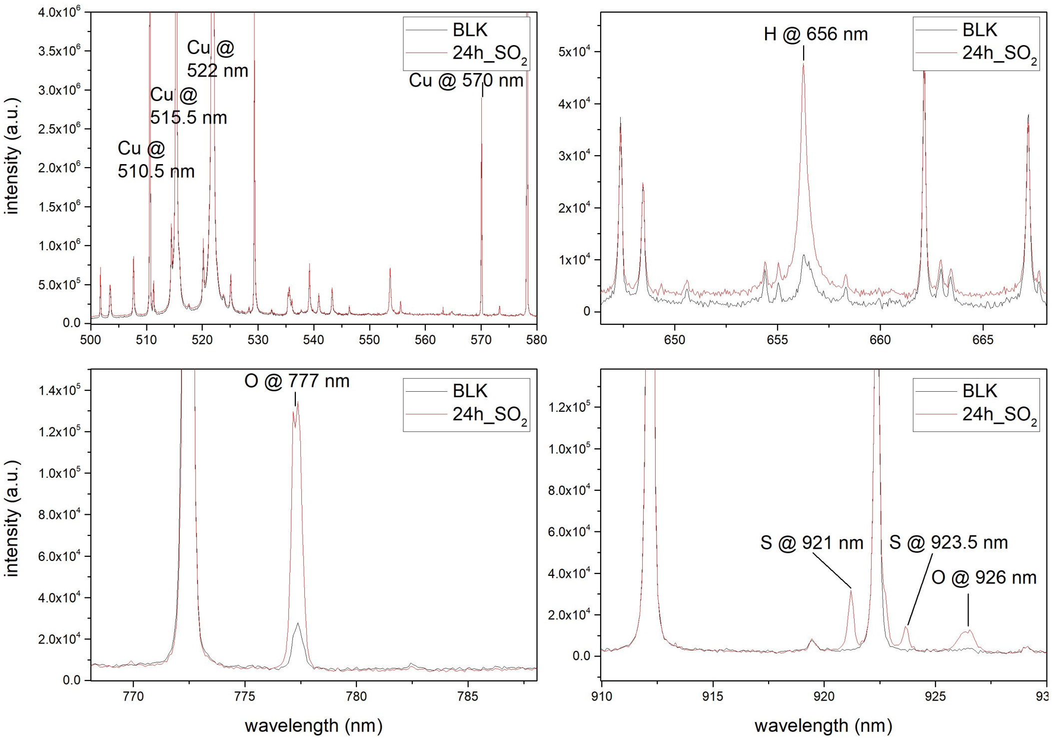

Figure 4.9.: selected emission lines of interest for the analysis of copper corrosion

should also be noted that, even for the Cu samples, only two emission lines, originating from the same transition, were observed for S. These two lines (S at 921 nm and 923 nm) are part of a triplet, but the center line is interfered by a strong Ar line. As the experiments were done in an Ar atmosphere the mentioned S line is only weakly visible as a shoulder and could not be used for data evaluation.

In figure 4.10 the evolution of the accumulated intensity of selected lines with increasing weathering duration is depicted. To give the qualitative results a more comprehensible meaning the data points shown in the graphs have been normalized to the value of the blank. This means that a y-value greater than 1 signifies an increase in intensity compared to the non-weathered sample. To obtain a more comprehensive view a dashed line has been drawn at $y = 1$. As only one sample was measured per weathering duration, no standard deviation of the accumulated signal could be calculated. Observed changes in the signal intensity thus have to be regarded with caution. However, a shift in the accumulated signal still signifies that the overall sample composition has been altered compared to the blank. In doing so, three interesting things can be noticed in figure 4.10:

1. The ratio for the depicted Ar lines remains close to 1. This is reasonable as the Ar emission is not expected to be significantly affected by the changes in surface composition.
2. The Cu emission line intensity slightly deviates from 1. The behavior of the H_2S samples (red squares) differs from that of the SO_2 (black squares). For the SO_2 samples hardly any difference in Cu signal was observed. The Cu line intensity of the H_2S samples is decreased by about a third. This is explicable due to the formation of corrosion products on the sample surface, which have a lower relative Cu content compared to pure copper. A possible reason why this effect is observed for samples weathered with H_2S only is discussed in the next point.
3. Looking at the graphs 3 to 6 (from left to right) in this figure, it becomes obvious that H_2S is the stronger corroding agent of the two. Firstly, the relative signal increase is higher in all cases. Secondly, for H_2S corrosion effects are already observable after 2 h, whereas the onset for SO_2 is after 3 to 4 h. It is worth noting that the increase in S signal is about tenfold the increase measured for the SO_2 samples, while it is

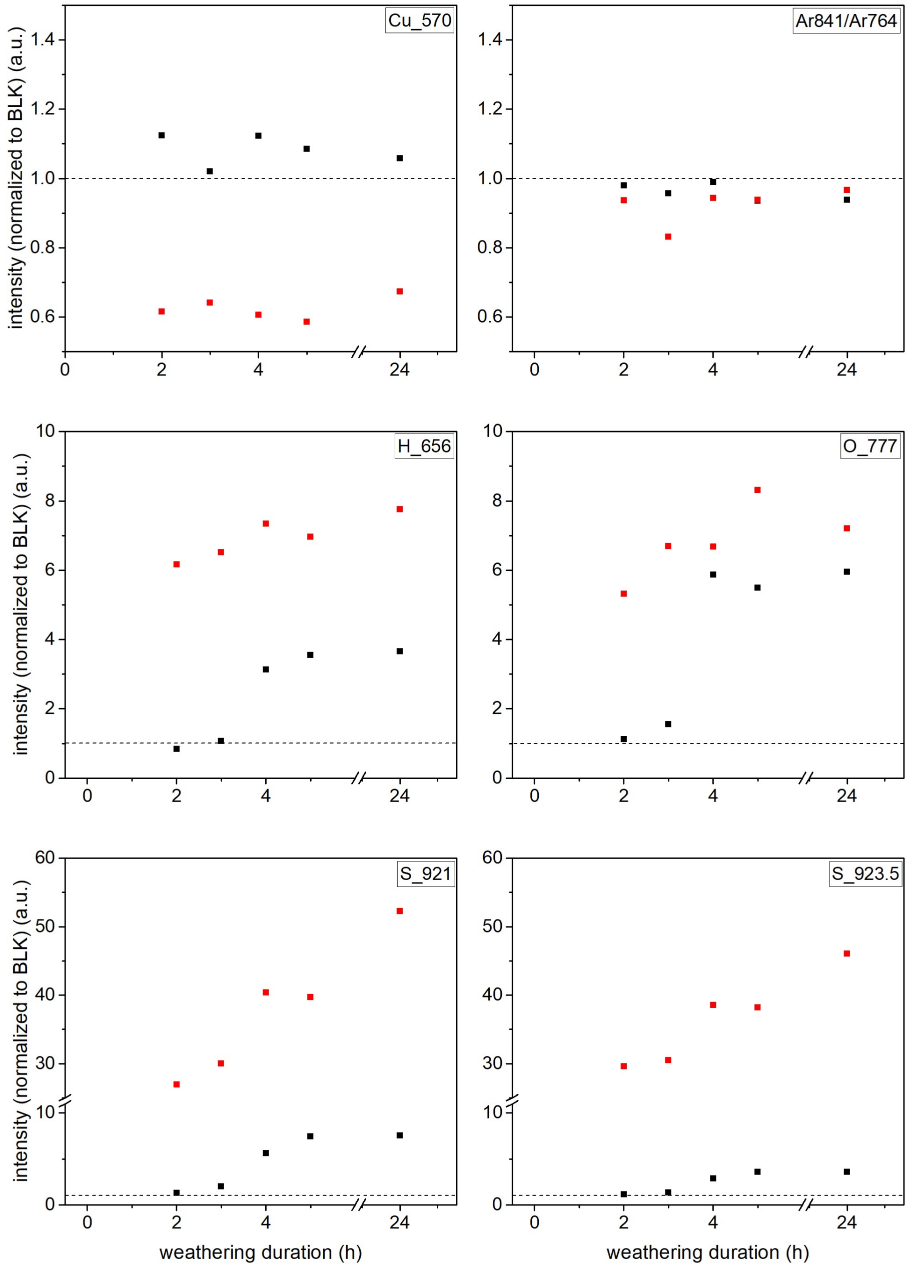

Figure 4.10.: evolution of selected emission line intensities depending on the weathering duration; red squares symbolize copper samples that were weathered in H_2S, black squares are copper samples that were weathered in SO_2; shown data points have been normalized to the intensity of the respective emission line of the blank (no weathering); the dashed line is drawn at y = 1

> only twofold or less for the H and O emission. One possible reason for the generally lower signal increase for H and O is the fact that, as seen in figure 4.9 the blank signal is already higher for these two compared to S. However, it is also indicates the formation of different corrosion products depending on the gas.

In the following figure (figure 4.11) microscopic images of the measured copper samples are shown, which support the LIBS results. Pictures C and D have been taken of samples that were weathered for 3 h in SO_2 and H_2S, respectively. While in image C barely any corrosion effects are observable, these are clearly identifiable in image D. In pictures E and F samples after 24 h in the weathering chamber (again SO_2 and H_2S, respectively) are presented. Here corrosion effects are visible for both samples. Yet in image E there is still some copper substrate visible, whereas this is not the case for image F.

4.2. LA-ICP-MS

As described in chapter 2.5.2 the measurement of S with LA-ICP-MS is less straightforward than it is for other elements. This proved to be right not only in theory but also during the practical work. As discussed in the theoretical part of this thesis (chapter 2.5.2), interferences due to oxygen, which is part of the chemical structure of PI (figure 2.2) strongly influence the measurement results for ^{32}S. One way that was attempted to overcome this problem was using a reaction cell as described in chapter 2.5.3. Oxygen was filled into the chamber as reaction gas to oxidize $32\,S$ to $32\,S_{16}O$. However, due to observed spectral interferences at mass 48 that were not distinguishable from the $32\,S_{16}O$ with the quadrupole's mass resolution, the attempt failed. Consequently, the decision was made to optimize the system for ^{34}S. The finally applied measurement parameters are depicted in table 3.4.

The first goal of the LA-ICP-MS measurements was to test the feasibility of using this technique for the investigation of polymer aging due to weathering and alteration or rather the interaction between polymer and corrosive gases/UV light in general. For this reason the initially conducted

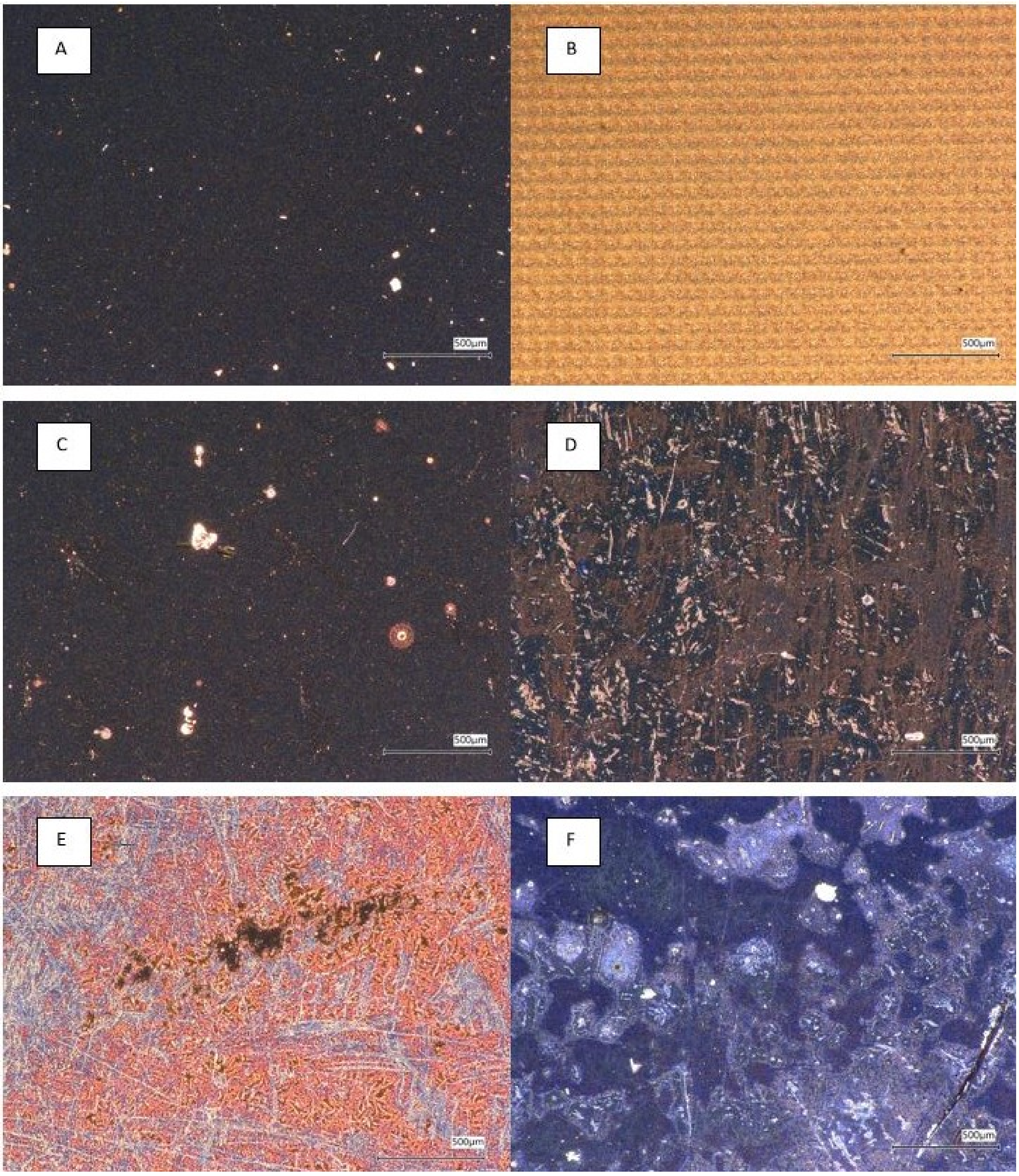

Figure 4.11.: microscopic images of various copper samples; A: pure Cu, B: Cu sample after LIBS ablation, C: Cu sample after 3 h of weathering with 50 ppm SO_2, D: Cu sample after 3 h of weathering with 50 ppm H_2S, E: Cu sample after 24 h of weathering with 50 ppm SO_2, F: Cu sample after 24 h of weathering with 50 ppm H_2S

measurements with this technique were spot measurements at 50 % laser energy, 5 Hz repetition rate and a beam diameter of 200 µm for 5 s, resulting in a total of 25 shots per spot. These spot measurements were performed on two of the PIs provided by partner from the industry, to be precise PI4 and PI5, after weathering with 50 ppm SO_2 for a variable time span. The aim was to test if weathering induced changes in the S content of the samples were measurable. For the five spots, which were distributed all over the sample, the measured signal was each summed up and the resulting sum was averaged. The obtained data is given in figure 4.12. In the graph the

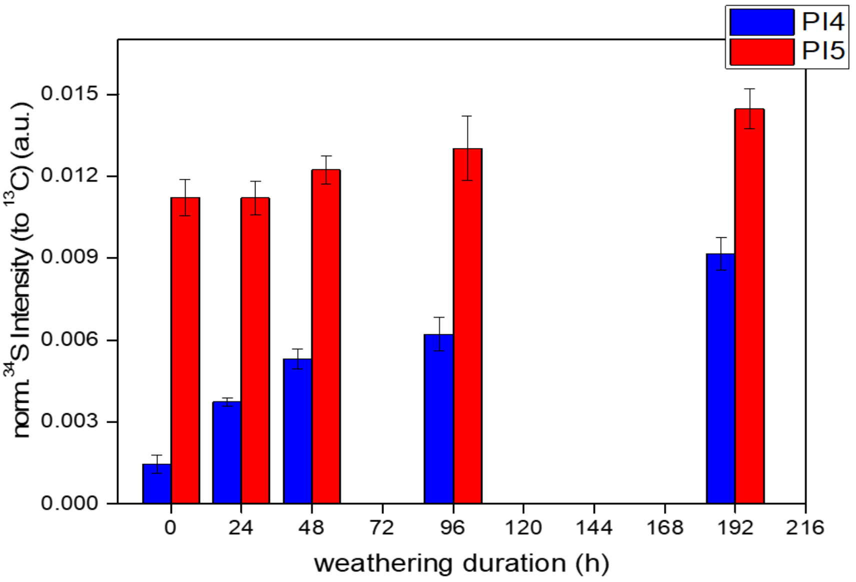

Figure 4.12.: LA-ICP-MS spot analysis of changes in total S content in PI4 (blue) and PI5 (red) after weathering for varying time spans in SO_2 enriched atmosphere

^{34}S signal, normalized to ^{13}C, is plotted against the weathering duration. ^{13}C was chosen as internal standard as carbon is part of the matrix and is assumed to be homogeneously distributed within each of the polyimide films. The normalization serves to compensate for instrumental fluctuations of the measured signal. A quick glance at the figure is sufficient to prove that, unlike with the LIBS, the LA-ICP-MS-system enables the measurement of changes in S concentration caused by the weathering. This is clear as for both PI4 and PI5 an increase in the total ^{34}S intensity is observable. It can

also be seen that the increase in relative S signal is higher for PI4 than for PI5, suggesting that the former has a higher S uptake. However, from this experiment it is not possible to determine the origin of the signal increase. This means that the S could be located anywhere in the PI film, only near the surface, (evenly) distributed all over the film or at the substrate.
Based on these findings the next goal was to establish a method with which depth profiles could be measured in order to clarify the S distribution in the PI. This was not possible with single shot measurements as the transient signal was too short. Hence, the next idea was to replace spot measurements by line measurements. This has two advantages:

- measuring a line results in a longer transient signal, which is more stable than single shot analyses and enables the identification of spikes. Also, especially for low signal intensities, a longer transient signal allows for better discriminability between background and analyte signal.
- measuring a line also leads to a loss of spatial information, which can be both an advantage as well as a disadvantage. If one is interested in the analysis of defects or the like spatial information is crucial. If however, as is the case for these measurements, bulk information is sufficient a line scan is advantageous as it resembles the bulk composition of the sample more closely than a single spot.

To test if line patterns work for depth profiling the PI4 sample that was weathered for 192 h was taken as it definitely showed an overall increase in S content compared to the blank. The result from this measurement in comparison to the blank is presented in figure 4.13. This graph demonstrates that it is possible to measure depth profiles of the S content in PI. At the same time it provides an answer to a question that remained unanswered from the LIBS measurements. It proves that S is not only able to penetrate the surface layer of the polymer but diffuses down to the substrate The depicted layer 13 is close to (few hundred nm) the substrate and an increase in ^{34}S signal is still definitely observable compared to the blank. One ablated PI layer in LA-ICP-MS measurements equals ≈400 nm (for more information see chapter 4.3).
To make sure that the measured depth profiles are reproducible also for different samples that were treated under the same conditions, a comparison of such samples was investigated next (figure 4.14). Two things are be

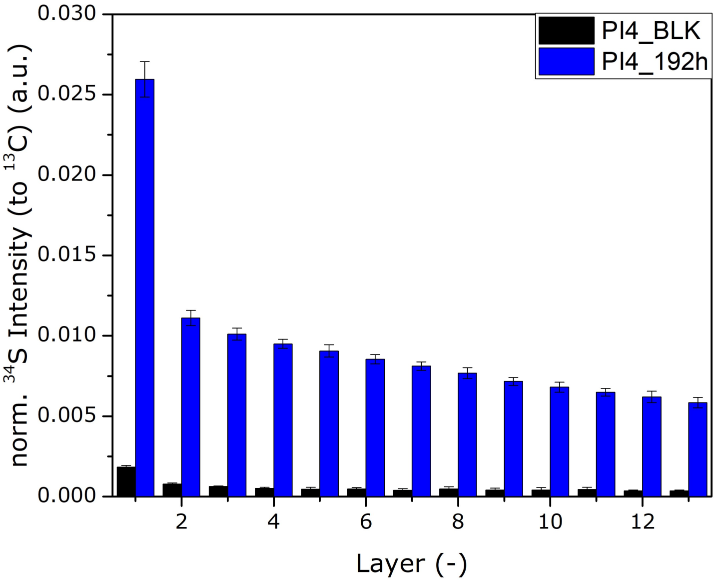

Figure 4.13.: exemplary depth profile of the ^{34}S content, obtained by repeated firing of a line pattern in the same area; the analyzed sample was PI4 after weathering in 50 ppm SO_2 for 192 h

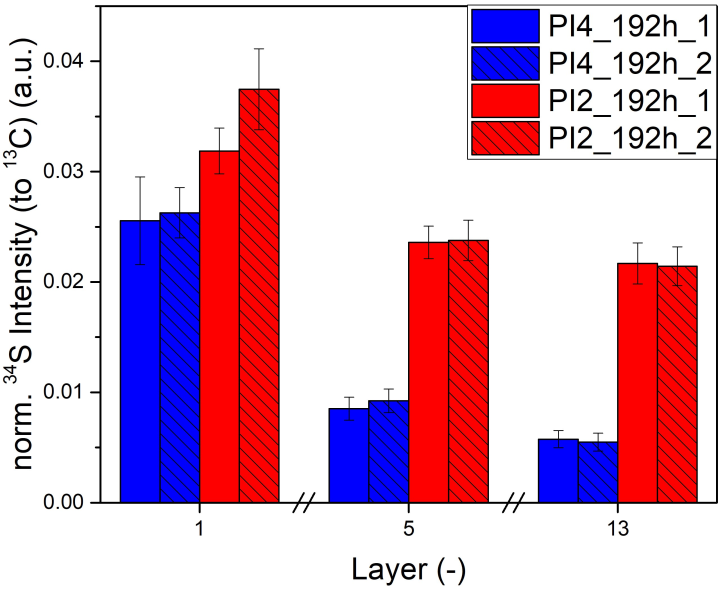

Figure 4.14.: exemplary investigation of S content of four different samples of two different PIs after treatment with the same weathering conditions (192 h SO_2)

deduced from this graph:

- In the first layer differences between the two samples of the same type are negligible for PI4 but relatively large for PI2. Variability in the observed value for this topmost layer might be due to surface contamination which adds to the S that is introduced due to the weathering with SO_2.
- While the samples partially differ in the first layer, the observed ^{34}S signal value is reproducible for all the other layers.

It is therefore concluded that the depth profiling based on line patterns has successfully been shown to be not only possible but also reproducible. Hence, from this point on experiments were done using a line pattern as described in chapter 3.3. The first of these measurements were done with the samples prepared in the earliest main weathering experiment (50 ppm of SO_2). Figure 4.15 contains data obtained from a blank and several weathered samples of PI4 and PI5. For both graphs the same scale was chosen. In doing so it is apparent that the relative signal increase is much higher for PI4 than for PI5. Additionally for PI4 a clear time dependence is observable. For this polymer, as time increases, an increase in ^{34}S signal was measured in the first and all consecutive layers. This implies that the PI is not saturated and would, upon increased weathering duration, absorb even more SO_2. For PI5 on the other hand no trend is apparent. Except for an increase in the

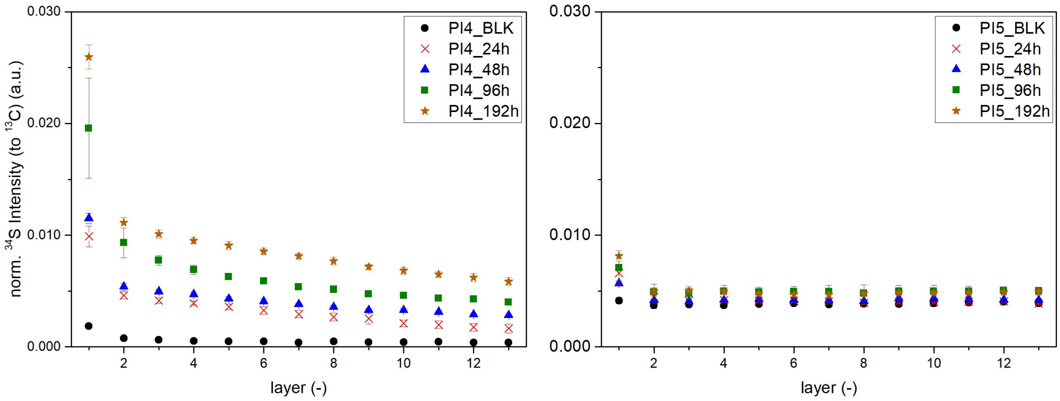

Figure 4.15.: comparison of PI4 (left) and PI5 (right), with varying weathering duration in SO_2 enriched atmosphere (50 ppm)

topmost ablated layer no significant change in S concentration was noticed. This suggests that PI5 is more resistant to SO_2 diffusion. However, as the results are qualitative only, a direct comparison of these two samples has to be done with caution, partially as the samples contain different amounts of "native" S based on their chemical structure. The results for all measured PIs are given in figure A.2 and the same data is rescaled to show the same scale for all measured PIs in figure A.3. These results will not be discussed here, as in a next step the data was manipulated in a way that eliminated the measured intensity of the native S.
This was done by subtracting the ^{34}S value measured for the untreated sample of PI from the ^{34}S value measured for the respective weathered sample. The idea here is to subtract the sulfur signal obtained due to native S out, leaving only the increase due to the weathering procedure. The results of all five PIs provided by the industrial partner are given in figure 4.16. After this mathematical manipulation of the data a value equal to zero signifies that no S was introduced to the polymer compared to the untreated sample. Numbers that are greater than zero mean an increase. In this figure it attention must be paid to the fact, that the y-axis is different for each of the five given graphs. This was done to better be able to see the dependence of the ^{34}S signal on the weathering duration for each of the PIs. From this figure a multitude of information can be extracted:

- At least a slight increase in ^{34}S signal intensity was measured for all PIs at all weathering durations even down to the substrate. Exceptions are found for 24 h and 48 h of weathering in the case of PI5 (graph E) and single values of PI1 (A) and PI3 (C). Again it has to born in mind that the scale is not the same for all of the samples.
- Due to the differences in scaling it can easily be read from the y-axes that in graph C, which depicts PI3, the highest increase in ^{34}S signal was observed, followed by D, B, A and E. The maximum increase was, not surprisingly, found for the sample with the longest weathering duration and in the first ablated layer.
- For graphs A, C and D a time dependence of the weathering is notable beyond doubt, for B and E this is less pronounced but for the average signal intensity there is also a grouping of 24 h and 48 h in comparison to 96 h and 192 h.
- In graph E, except for the first layer, a uniform distribution of intro-

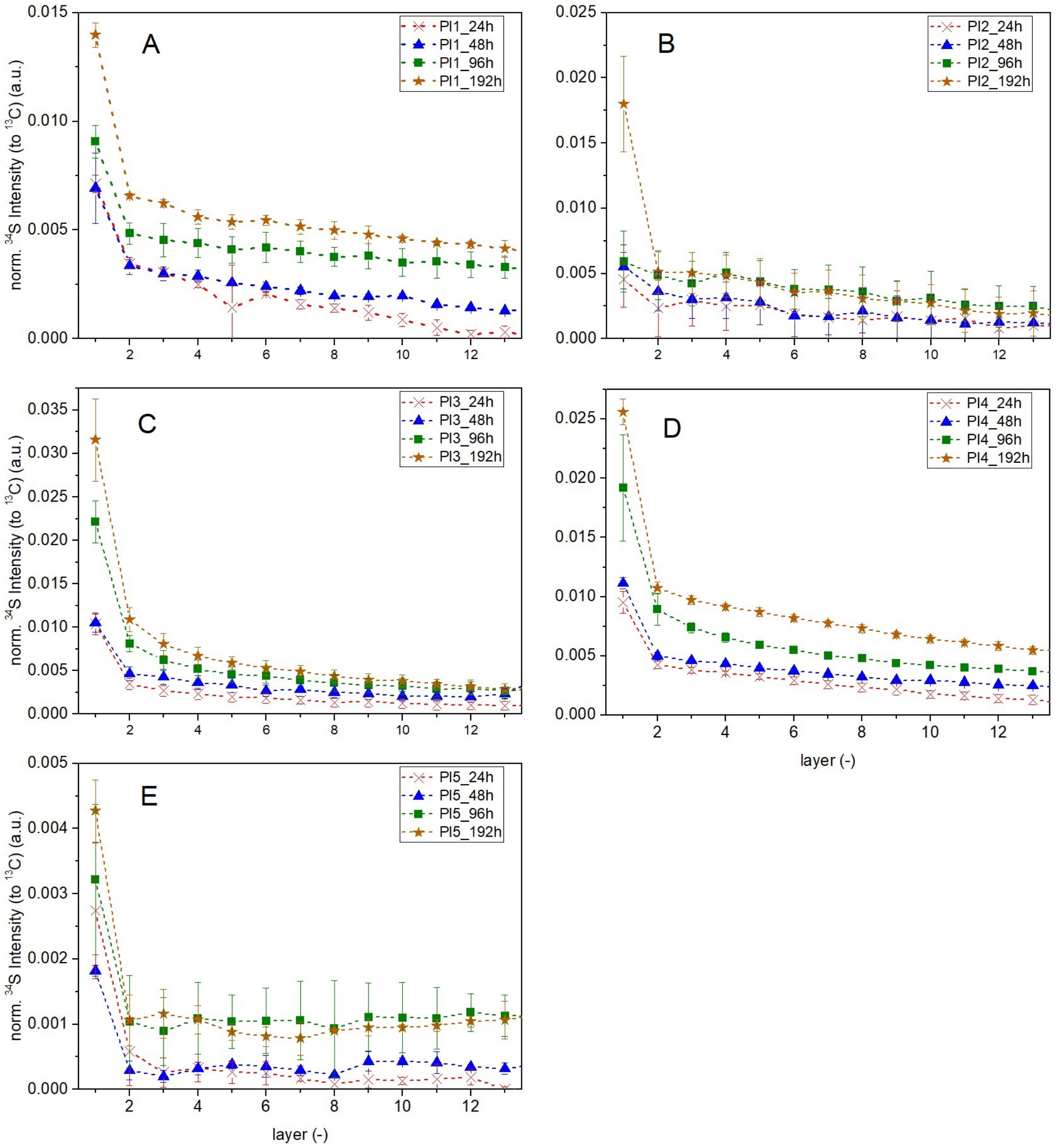

Figure 4.16.: development of normalized ^{34}S signal with increasing sampling depth at different weathering duration in 50 ppm SO_2 for PI1 (graph A) to PI5 (graph E); the normalized ^{34}S signal of the respective blank has been subtracted from the values obtained for the weathered samples of the PIs

duced S was measured. This is, however, most likely attributable to the generally low increase in ^{34}S signal intensity.

In order to compare the polyimides to one another more easily, figure 4.17 was created, for which the samples that were weathered for the maximum amount of time (192 h) were picked out and plotted. Here the previously made observations are confirmed and variations in the lower layers of the polymer are more clearly visible. In the case of PI1, for example, it is notable, that this polymer yielded a lower ^{34}S signal increase in the first layer compared to PI3, but down to the substrate this changes, as the slope for PI1 is less steep than for PI3.

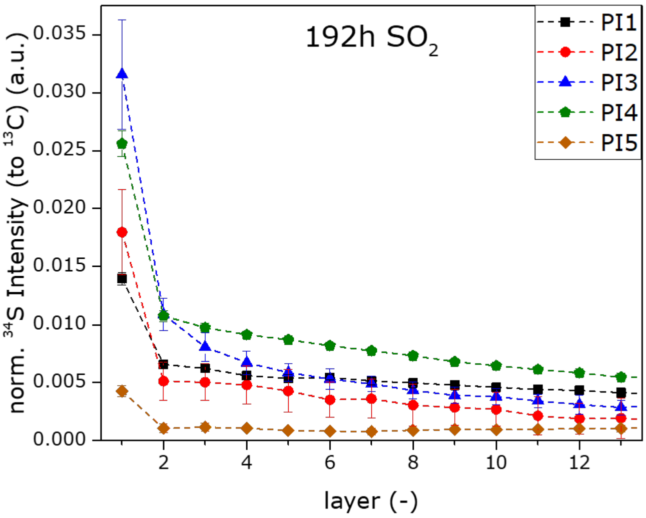

Figure 4.17.: comparison of all five PIs, weathered for 192 h in SO$_2$ enriched atmosphere (50 ppm)

Overall, based on the results from the SO$_2$ weathering measurement series, PI5 would be the best suited polymer as protective film for microelectronics with regards to the barrier properties against SO$_2$, both on short as well as long terms. These differences originate from a variety of causes. As diffusion processes depend on the Langmuir and Henry absorption of the polymer, as described in chapter 2.2.2, the barrier properties clearly depend on the basic chemical structure, the degree of cross-linkage and other factors. The cross-linkage in turn depends on, e.g., the curing process, which means that also the preparation of the polymer plays an important role with regard to the final properties. Another possible explanation for observed differences in the permeability would be measurement of a, sort of, false positive. This means that it is possible that the point of time at which the sample was measured, compared to the rest of the samples, has an influence on the result. It was not possible to measure all samples in one day. Thus, if diffusion out of the sample occurred in the meantime (during storage of the previously weathered samples) the results for one PI might be lower than those measured for the prior investigated PI. To determine whether this effect occurred or not the same sample was measured twice, one week apart. In between the two measurements the samples were stored in the laboratory in plastic boxes (article number: 47410-0101, Bock GmbH & Co. KG, Lauterbach, DE) under ambient conditions. The resulting data is presented in figure 4.18. These measurements show that differences due

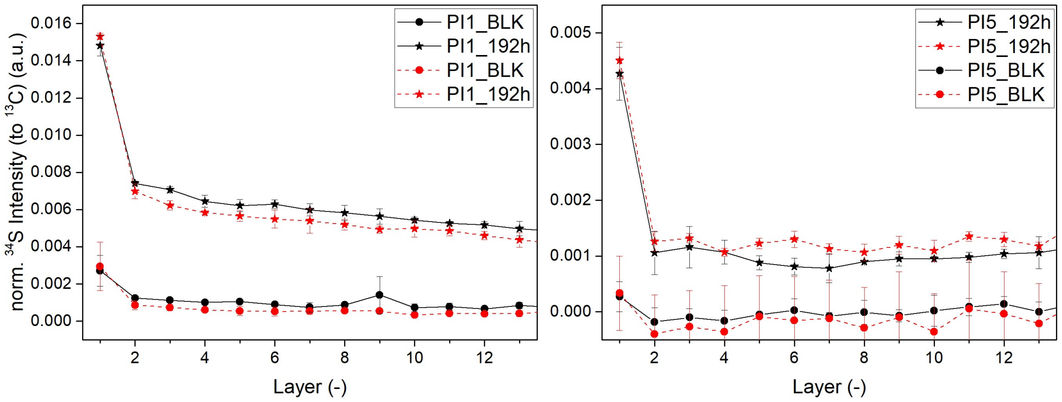

Figure 4.18.: comparison of measurement results for PI1 and PI5 weathered with SO_2; black and red measurement results were obtained from the same samples (left: PI1; right: PI5) and under the same conditions (boxed, ambient conditions) but measured one week apart to test the influence of storage time on the (weathered) samples; results shown in black were measured prior to samples in red

to the storage are small to negligible. Still, all measurement series were conducted within a maximum of one week's time relative to one another. After the weathering experiment with SO_2 the second series with 50 ppm

H_2S was conducted and investigated. As it is known from literature and was affirmed in chapter 4.1.2 H_2S is the more critical corrosive agent compared to SO_2 when it comes into contact with metals. This makes the study of the diffusion into the polyimide film especially interesting.
The results obtained from the LA-ICP-MS measurements of the samples that were weathered for 192 h in H_2S are depicted in figure 4.19. As was done for

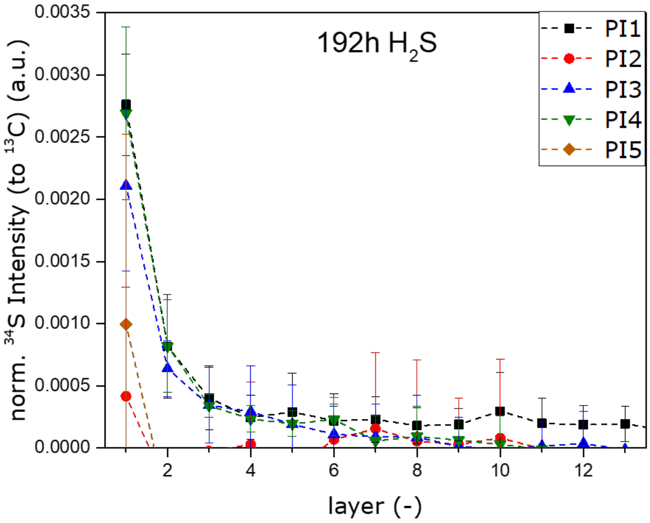

Figure 4.19.: comparison of all five PIs, weathered for 192 h in H_2S enriched atmosphere

the SO_2 samples, the signal intensity obtained due to the native S was once again subtracted. The maximum observed ^{34}S value due to weathering with SO_2 was ≈ 0.032 a.u.. The investigation of H_2S yielded a maximum value of $\approx 0.002\,75$ a.u., which is more than a factor ten less. The highest values were obtained for PI1 and PI4, the lowest for PI2, followed by PI5. Relative standard deviations of the results are much higher in these cases than they were in the previous measurement series, this is at least partially caused by the low overall increase in ^{34}S signal intensity compared to the native S. It is curious that all samples, except PI1, show no significant S uptake in the case of H_2S. Even for PI1 the deviation from zero is only visible due to the chosen scale on the y-axis. The observed results are unexpected as the kinetic diameters of the two gases are the same (chapter 2.2.2). The size can therefore not be the reason for the observed discrepancy. Differences in polarity are thus most likely to explain the deviating results. Oxygen is more electronegative than sulfur, but the latter is more electronegative than hydrogen (table 4.1). Hence, in SO_2 sulfur is positively polarized, whereas in the case of H_2S the S pulls electrons towards itself and is negatively polarized. This can strongly influence the interaction between polymer and gas. Although unexpected, it is a welcome finding that all of the PIs have a higher resistivity against diffusion of H_2S into the film and thus to the substrate than was observed for SO_2. Although for many samples no, or at least barely any, signal increase was measured this does not necessarily mean that no H_2S successfully penetrated the polymer film at all. It is still possible that minor changes under the limit of detection of the used method occurred. However, from the measured data it is undeniable that SO_2 uptake is a lot higher than that of H_2S. For determination of the limit of detection as well as a practical meaning of this difference, quantitative analysis is necessary. As described in chapter 2.3.3 there is no straightforward method to this for solid samples and it was not successfully done within the scope of this thesis. In figure A.4 in the appendix the H_2S plot shown above (figure 4.19) is rescaled to the same scale used for the SO_2 samples. This allows for an easier comparison of the two weathering experiments and the resulting ^{34}S signal intensity increase.

Table 4.1.: electronegativities of selected elements (H, O, S) based on the electronegativity scale by Allred and Rochow; numbers taken from Huheey (1997)

element	**electronegativity** (Å^{-2})
H	2.20
O	3.50
S	2.44

Since the results from the H_2S samples showed good resistivity of the PIs against H_2S diffusion the decision was made to step up the aggressiveness of the experimental set-up. Therefore another experiment was conducted for which a UV exposure step was added prior to the weathering with H_2S. This way the effect of alteration prior to the weathering was sought to be determined. In figure 4.20 the results for the samples with the maximum UV exposure as well as the maximum H_2S weathering duration are plotted.

The obtained graph clearly differs from the graph that was previously

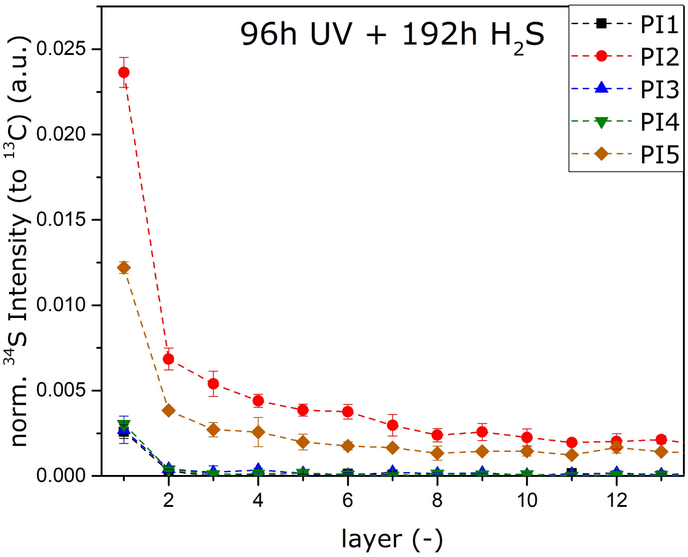

Figure 4.20.: comparison of all five PI, exposed to UV for 96 h and weathered for 192 h in H_2S enriched atmosphere

shown (figure 4.19). This indicates that UV exposure influences the uptake of H_2S into the polyimide. For PI1, PI3 and PI4 the 96 h UV exposure prior to the weathering do not seem to make any difference compared to the weathering alone. Their values lie at around 0.0025 a.u. as was observed before. However, this is not true for the other two polyimides, PI2 and PI5, which were the most resistant in the previous experiment. Although no changes were measurable with the LIBS set-up, it becomes clear from the MS data that the UV exposure did affect these two PIs and lead to a significant signal increase. Minor changes in the polymer structure might not allow for a distinction between altered and non-altered sample when doing LIBS measurements, but possibly result in an “activation” of the surface (e.g. by breaking of bonds). The activated surface is then more reactive and absorbs an increased amount of H_2S. As the chemical structures of the PIs differ not all of them are affected in the same way. For both of the polyimides that were impacted by the UV exposure the increase in ^{34}S signal intensity was highest in the first ablated layer but not restricted solely to it. Also for these two samples a slight increase was observable down to the surface. Like before in the case of H_2S weathering, in figure A.5 in the appendix the UV plot shown above is rescaled to the same scale used for the SO_2 samples. As an increase in ^{34}S signal was observed in the case of the UV exposure prior to the weathering, it is interesting to look at possible trends in the signal evolution depending on a change in UV exposure time. Figure 4.21 shows two graphs with the corresponding data. As no significant increase in

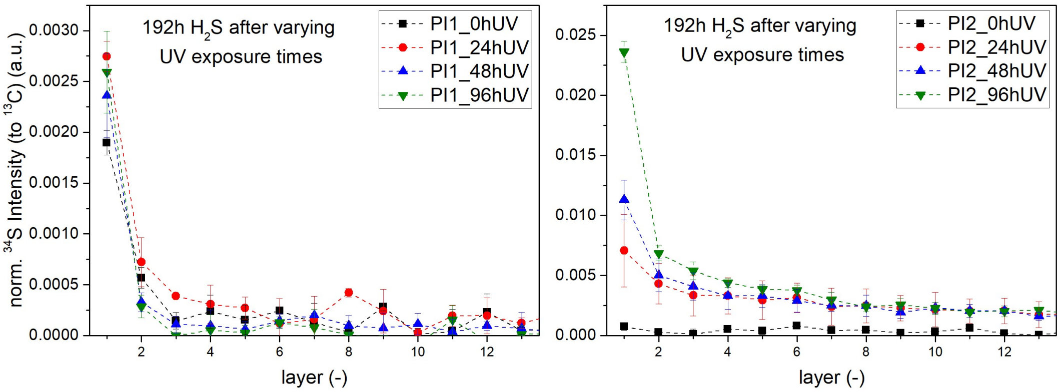

Figure 4.21.: comparison of PI1 (left) and PI2 (right), with varying UV exposure times and weathered for 192 h in H_2S enriched atmosphere (50 ppm H_2S)

^{34}S signal intensity was found after 96 h of UV exposure it is not surprising that no time dependence is observable for PI1 (left graph). For PI2 (right graph), which had the highest increase after the maximum UV exposure, a clear trend is observable. 96 h of UV exposure result in the highest signal increase, followed by 48 h and 24 h. However, this trend seems to be limited to the upper layers and is not notable in the lower layers, although compared to the blank there is still a signal gain. At first sight, in figure 4.22 one makes an observation that is quite similar to the results discussed for PI2. However, in this case the order is a bit jumbled, as the measured signal increase is higher for the sample that was exposed for 24 h compared to the 48 h exposure. With only one measured sample it cannot be said whether this result is reproducible. Still, it can be assessed that for PI5 a time dependence is given, although it might be less simple than the one in PI2.

In the final figure of this chapter (figure 4.23) a wafer that was used in the last experiment only, namely one with a protective layer of PI1 atop a copper substrate ("W19"), is plotted. This figure is different than the previously presented ones for two reasons. Firstly, two y-axes (left: ^{34}S signal

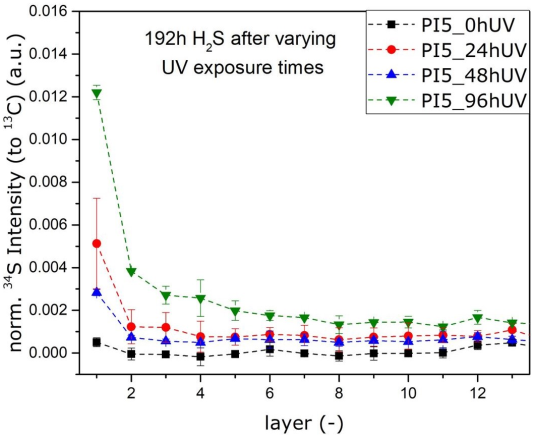

Figure 4.22.: depiction of PI5 with varying UV exposure times prior to weathering for 192 h in H_2S enriched atmosphere (50 ppm H_2S)

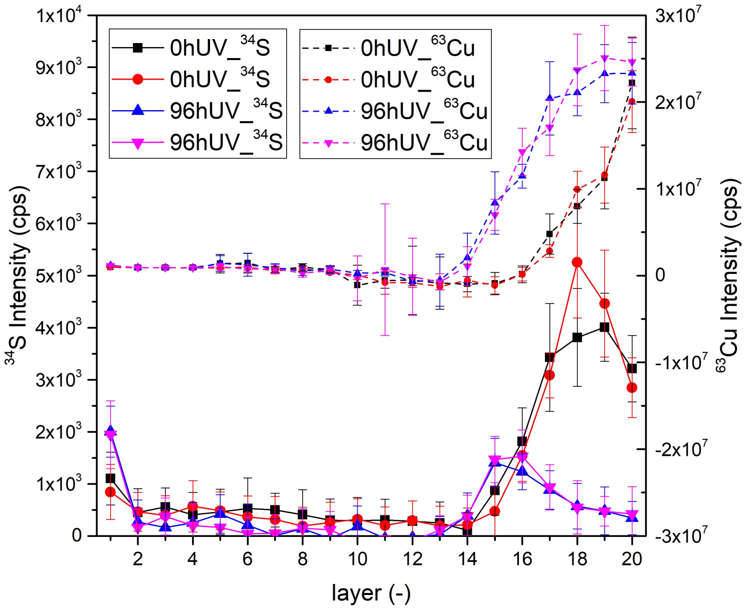

Figure 4.23.: depiction of ^{34}S (left y-axis) and ^{63}Cu (right y-axis) signal intensity of samples cut from a wafer with copper substrate; as for the previous graphs the blank signal was subtracted from the depicted data; presented are: 0 h UV exposure and 192 h weathering in 50 ppm H_2S (black and red), 96 h UV exposure and 192 h weathering in 50 ppm H_2S (blue and magenta)

intensity, right: ^{63}Cu signal intensity) are pictured. Secondly, the ^{34}S signal is not normalized to ^{13}C. The latter is due to the fact that the aim of this measurement was not, as before, to analyze the diffusion into the polyimide, but to see if the ^{34}S signal increased at the interface between polymer and copper. In this case a normalization does not make sense as it would falsely lead to an increase in the normalized signal as soon as the substrate is hit, as the matrix changes from polymer to copper. The ^{34}S diffusion normalized to ^{13}C was not of interest here as it has already been discussed for PI1 at earlier stages in this chapter.
In the figure it is apparent that in the topmost layer (of the polyimide film) the ^{34}S signal is slightly increased for the UV exposed samples compared to the non-exposed samples, as was observed for PI1 in the aforementioned experiments. Looking at the right end of the y-axes one thing catches one's eye immediately. The sample is penetrated earlier (after 14 layer) in the case of the UV exposed samples compared to the non-exposed ones (16 layer). This indicates an influence of the UV exposure on the ablation which should be examined in future experiments. A second insight that is remarkable is that the gain in ^{34}S signal intensity at the substrate is higher for the H_2S samples without prior UV exposure. It is possible that this reduction in permeability can be explained by a densification of the PI film due to the irradiation, which leads to chain relaxation and consequently results in a decrease of $C'_{H,i}$ (see chapter 2.2.2). This was observed by Matsui, Ishiguro, et al. (1997) and Matsui and Nakagawa (1998), though not for H_2S. However, this does not explain why the UV exposure results in an increase in the topmost polymer layer. Therefore, although interesting, this was only the first measurement with this type of sample and the results should be regarded with caution and leave open questions that go beyond the scope of this thesis.

4.3. Profilometry

As the term "layer" has no physical meaning by itself, profilometric measurements were performed to determine the ablation depth per laser pulse for LIBS and LA-ICP-MS measurements. An exemplary result for a corresponding LIBS measurement of PI1 is given in figure 4.24. It is visible

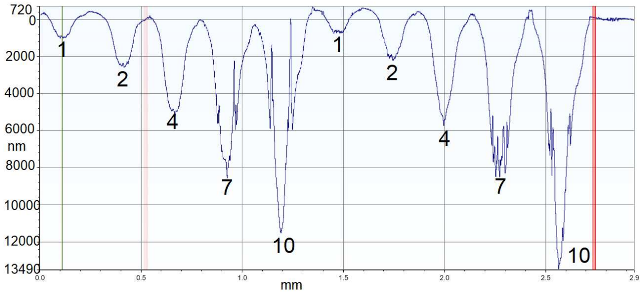

Figure 4.24.: exemplary profilometric measurement of PI1 after pulsing with the LIBS laser (266 nm); the numbers written underneath the crater represent the number of laser pulses

from this plot that the average ablation depth of a single pulse is >1 µm (≈1200 nm). This matches the observation that, for LIBS measurements, at the sixth ablation pass the substrate was laid bare. In the case of the copper samples without PI protection the ablation per pass was found to be ≈800 nm.

Profilometry was also used to examine the ablation per LA pass with the 213 nm laser. Due to the lower chosen laser energy coupled with a bigger spot diameter and a generally lower energy output for this laser compared to the 266 nm Nd:YAG, the strongly reduced ablation depth, as seen in figure 4.25, is not surprising. The calculated average ablation depth is <400 nm (356 nm). In figures A.6, A.7, A.8, A.9 and A.10 in the appendix profilometric maps of all five PIs provided by the industrial partner are presented.

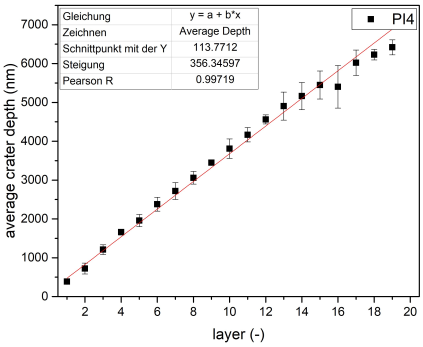

Gleichung	y = a + b*x
Zeichnen	Average Depth
Schnittpunkt mit der Y	113.7712
Steigung	356.34597
Pearson R	0.99719

Figure 4.25.: regression line obtained from profilometric measurements of craters in PI4; pulsing was done with the 213 nm laser used for LA

5. Conclusion and outlook

The aim of this thesis was to test the feasibility of two laser based analytical techniques for the measurement of weathering and UV exposure induced effects on polyimides and copper. Special focus was on sulfur-containing corrosive gases. The methods of choice were LIBS and LA-ICP-MS.

Three major weathering experiments, based on the results of preliminary experiments, were performed. These included weathering with SO_2, weathering with H_2S and, third and last, UV exposure prior to weathering with H_2S. One commercial PI, five PIs provided by a partner from the industry and pure copper were subject to examination.

With LIBS it was possible to detect alteration of some PIs due to UV irradiation. Measurement of depth profiles was accomplished. Also the qualitative measurement of corrosion products formed on the surface of bare Cu due to weathering with SO_2 and H_2S was successful. However, measurement of weathering effects in PIs did not work out.

PCA proved to be a powerful tool for multivariate analysis, which allowed the inclusion of a lot of spectral information rather easily. Also, once spectral descriptors were established it was a quick way to determine if a PI was significantly changed by the UV exposure. It was found, that PI2 and the commercially available P84 were most sensitive to UV exposure.

Analysis of corrosion products on Cu was successful and confirmed the visual observation, that H_2S has a higher corrosion rate on copper when compared to SO_2. This was found due to the onset of measurable corrosion effects and the relative intensity increase.

For LA-ICP-MS the measurement of ^{34}S in PI was optimized. Measurement of ^{32}S was neglected due to interferences with $^{16}O^{16}O$. The oxidation of ^{32}S to $^{32}S^{16}O$ by using a reaction cell filled with oxygen was also not possible due to spectral interferences. Consequently, ^{34}S was chosen as analyte of interest.

Doing so, examination of diffusion of sulfur into the polyimides was accomplished by measuring depth profiles. The results from the weathering experiments showed that the amount of SO_2 permeating the PIs is a lot higher than (factor of ≈10) that for H_2S. Except for the topmost layer, hardly any increase in ^{34}S signal intensity was observed in samples that were weathered with H_2S. On the other hand, samples that were weathered in an atmosphere that was rich in SO_2 clearly showed a signal increase and differences between the examined PIs were observed. PI5 proved to be most resistant to SO_2 uptake, whereas PI3 and PI4 had the strongest signal gain. Though less high, a signal increase was measured even in the layers close to the substrate. Also a time dependence of the sulfur diffusion was observed with SO_2 weathering. The low signal gain seen in H_2S samples does not necessarily mean that no sulfur permeates the polymer film, but the changes are close to or at the limit of detection and the concentration increase is definitely less than in the case of SO_2.

The third experiment which included UV exposure prior to the H_2S weathering revealed that UV irradiation influences the permeability of the gas in the PI. Unlike in the case of solely weathering with H_2S, in the third experiment PI2 and PI5 yielded increased ^{34}S intensity values which were similar to the ones observed for weathering with SO_2. The other three PIs remained unaffected. In the case of PI2, a trend was found that rising UV exposure time results in increased ^{34}S signal intensity. For PI5 the influence of UV exposure is also given but determination of the time dependence is harder.

A first measurement of a sample that was also covered with PI but had a copper substrate suggests that diffusion of H_2S down to the sample is higher in samples that are not exposed to UV irradiation. This opened up many new questions which will need further investigation.

As the feasibility, capabilities and limitations of LIBS and LA-ICP-MS have been assessed, a multitude of additional experiments would be of interest to retrieve more comprehensive insights.

First of, new weathering experiments can be designed, with variations of RH, new gaseous species (e.g. O_3), combinations of gaseous species (e.g. SO_2+o_3) or simply increased weathering and exposure duration. In these experiments samples with a copper substrate underneath the PI film should be integrated.

The currently employed weathering chamber does not allow for variation of the temperature or application of a current. If this non-availability was removed, those two parameters could also reveal important new insights, especially in combination with the aforementioned parameters.

Lastly, special effort should be made towards development of a method for quantitative analysis, both for PI and Cu. This was not managed within the scope of this thesis. A possible approach for the latter has thoroughly been described by Ludwig (2014). Ideas for quantification in polymers are extractable from chapter 2.3.3 and references therein.

A. Appendix

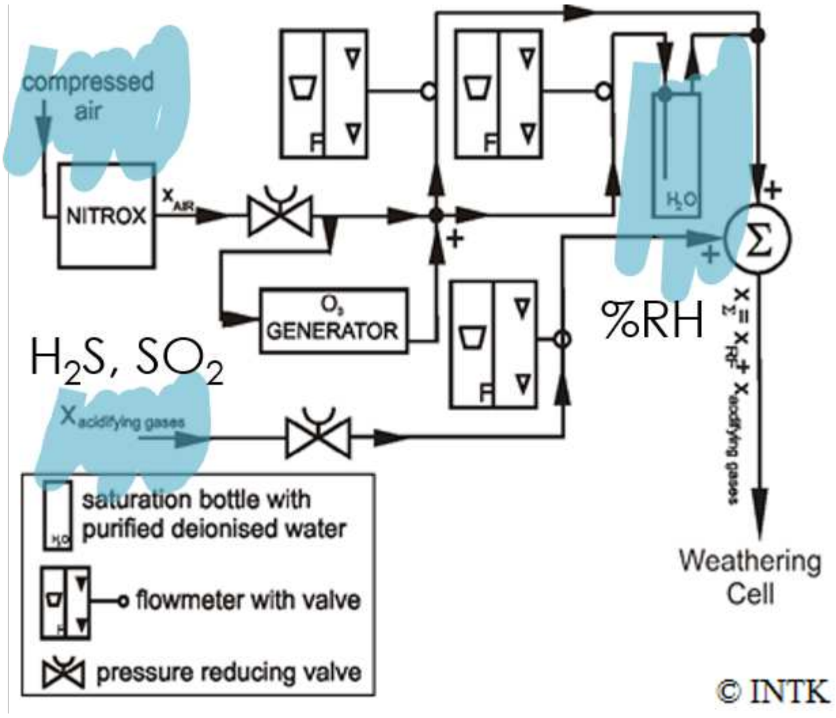

Figure A.1.: Laboratory test exposures: weathering experiments - schematic of the gas mixing set-up, with permission from Dipl.-Ing. (FH) Dr.techn. Priv.-Doz. Rita Wiesinger, Academy of Fine Arts Vienna

Table A.1.: UV chamber: product information and figures of merit

name	producer	source of light	irradiance Wm^{-2}	radiation nm
UVACUBE SOL 2/400 F	Dr. Hönle AG UV-Technology, Germany	Xenon arc lamp	910	295 - ≈3000

Table A.2.: used spectral descriptors for calculation of PCAs from LIBS data for PI; letters symbolize the source of the emission, numbers in the table indicate the lower and upper end (wavelength in nm) of the selected spectral area

C	C	CN	CN	undefined source	undefined source	C2
192.7	247.3	357.9	384.6	419.0	435.7	467.3
193.4	248.8	359.6	387.3	421.9	438.4	473.9

C2	C2	C2	C2	C2	C2	undefined source
466.4	506.9	516.7	530.9	551.8	563.8	604.9
473.9	513.2	513.2	563.9	558.7	558.7	619.6

H	Ar	Ar	Ar	O	C	Ar
651.5	696.1	705.9	736.5	776.2	833.2	840.1
659.9	697.8	708.2	774.8	778.4	834.1	843.1

Ar	Ar	C	C	C	C	Ar
851.6	866.6	905.6	907.5	908.6	910.9	911.7
852.9	867.2	907.1	908.4	910.8	911.7	913.2

Ar	C	C	C
922.1	940.1	961.9	965.4
923.5	941.3	962.5	966.3

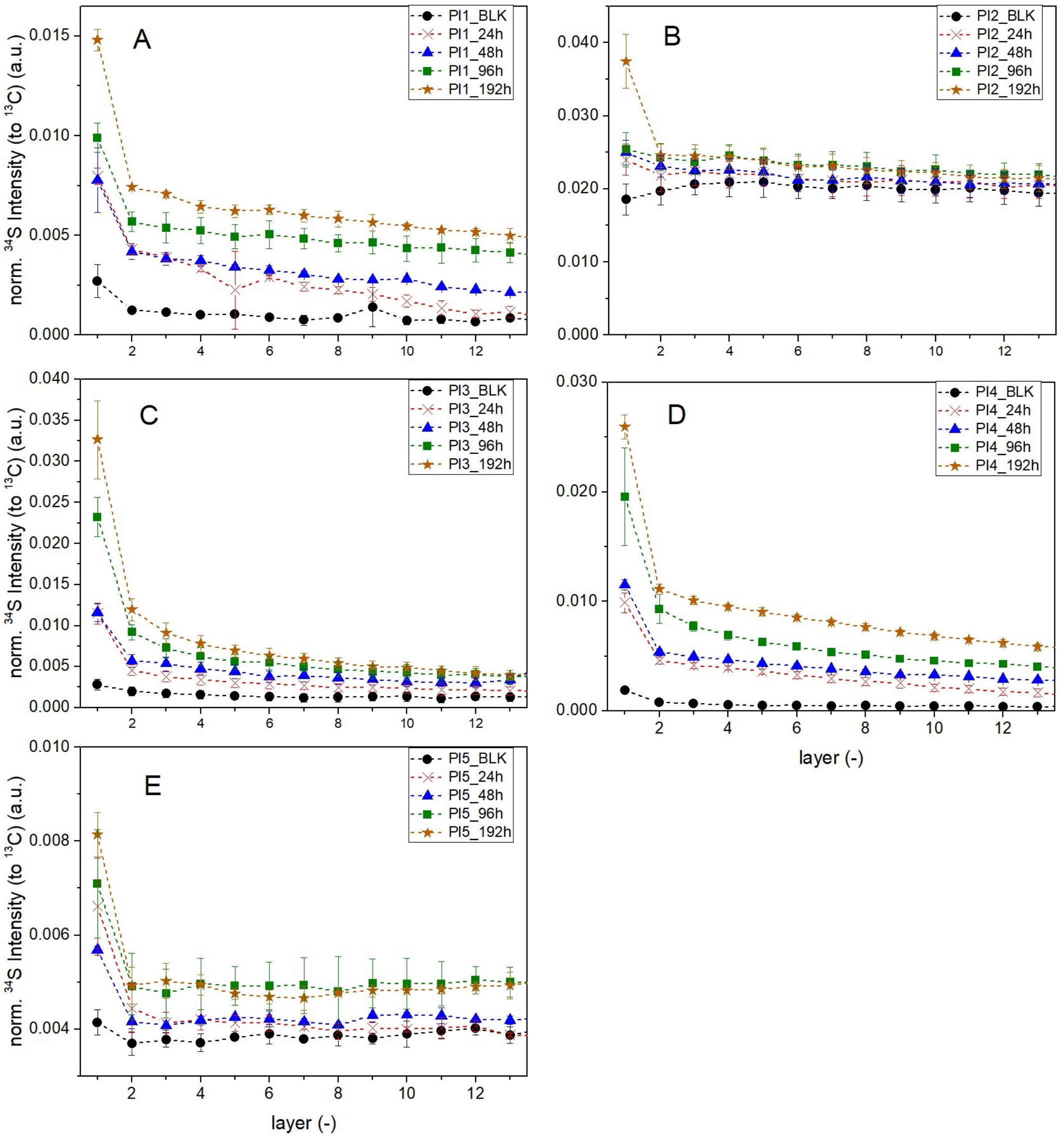

Figure A.2.: development of normalized ^{34}S signal with increasing sampling depth at different weathering duration in 50 ppm SO_2 for PI1 (graph A) to PI5 (graph E); see figure A.3 for comparison of the data in this figure with the same scale for all PIs

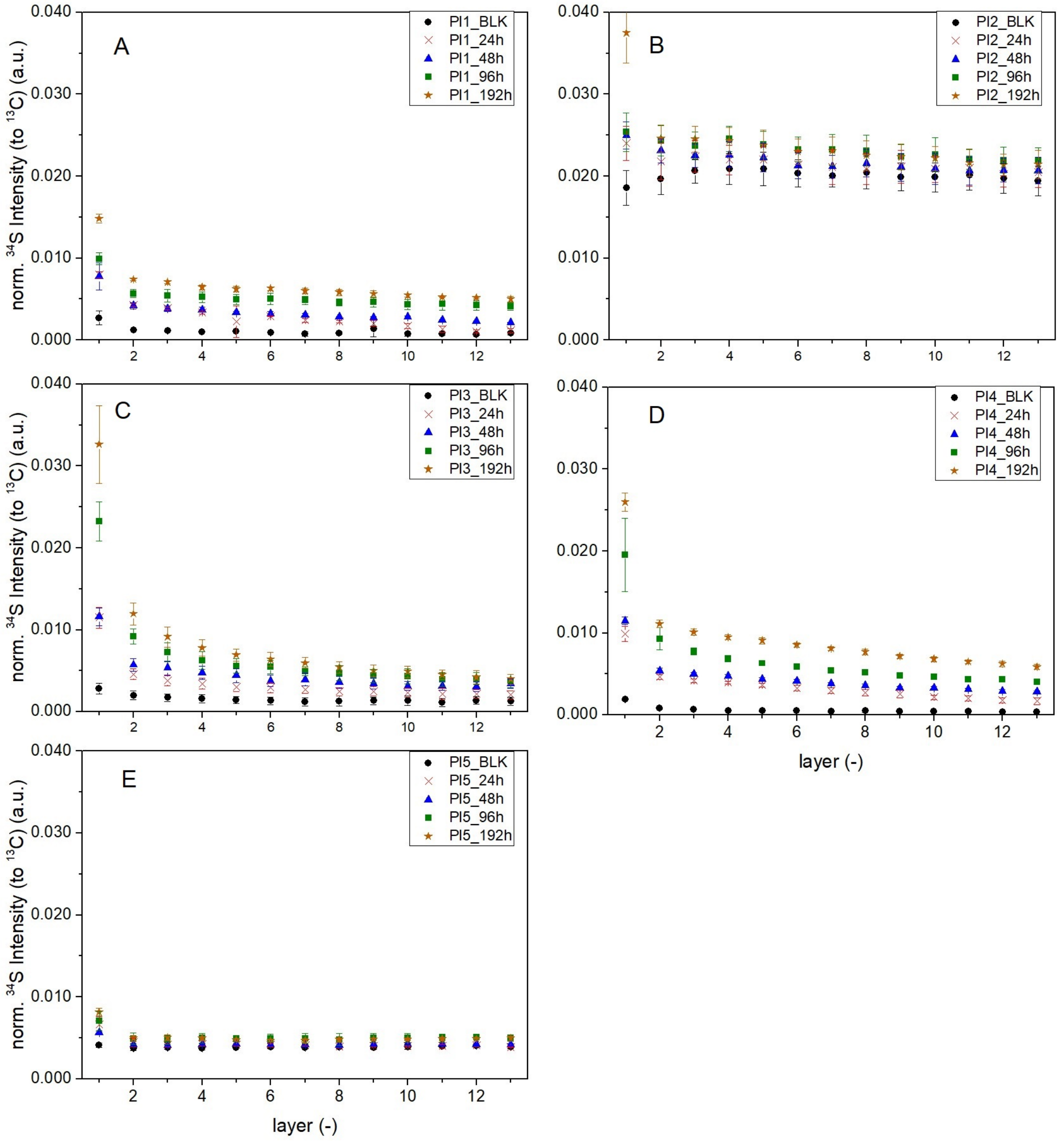

Figure A.3.: development of normalized ^{34}S signal with increasing sampling depth at different weathering duration in 50 ppm SO_2 for PI1 (graph A) to PI5 (graph E); the data is the same as in figure A.2 but the same y-axis scaling was chosen for all PIs

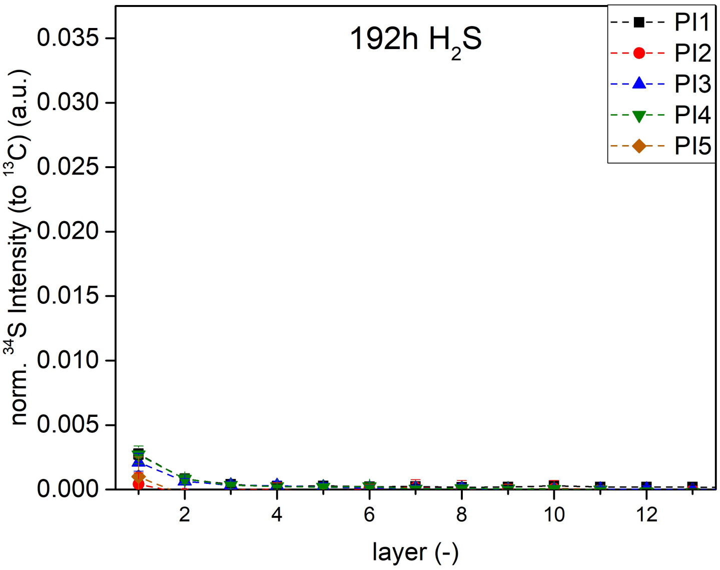

Figure A.4.: comparison of all five PI, exposed to UV for 96 h and weathered for 192 h in H_2S enriched atmosphere, rescaled to the scale used for SO_2 (figure 4.17)

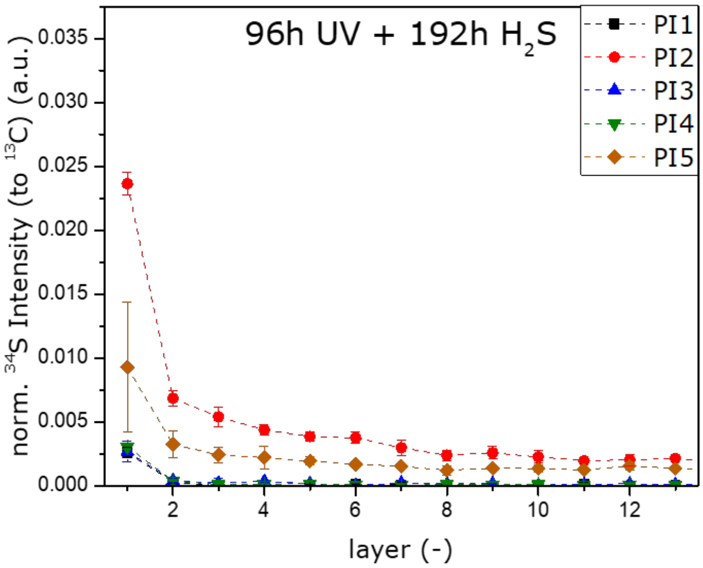

Figure A.5.: comparison of all five PI, weathered for 192 h in H_2S enriched atmosphere, rescaled to the scale used for SO_2 (figure 4.17)

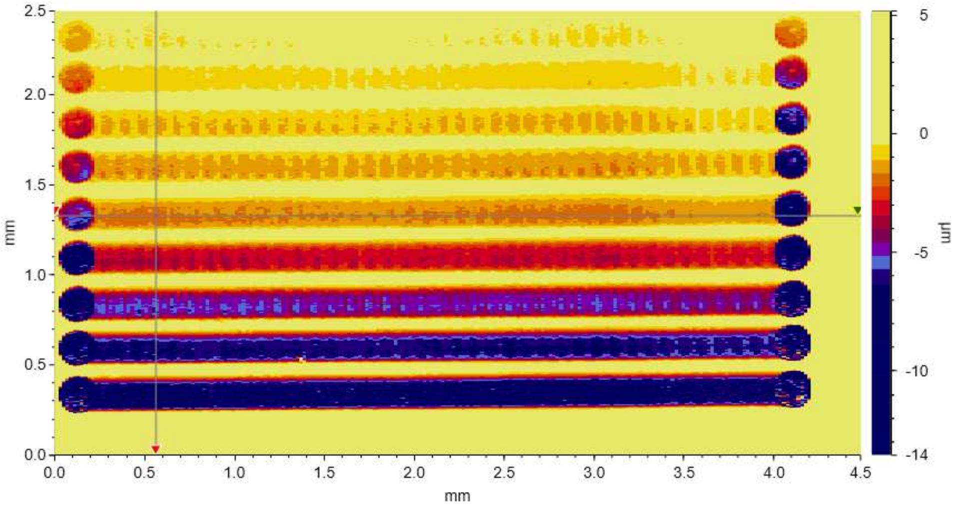

Figure A.6.: profilometric measurement of PI1; craters were obtained from LA-ICP-MS measurements; the number of pulses per crater were (from top to bottom): 1, 2, 3, 4, 5, 10, 15, 20, 25

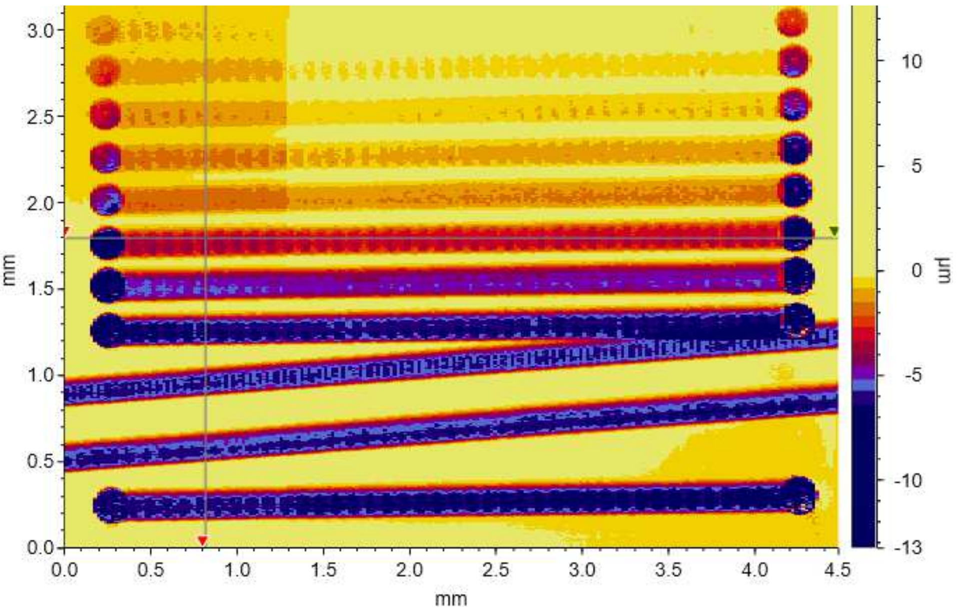

Figure A.7.: profilometric measurement of PI2; craters were obtained from LA-ICP-MS measurements; the number of pulses per (parallel) crater were (from top to bottom): 1, 2, 3, 4, 5, 10, 15, 20, 25

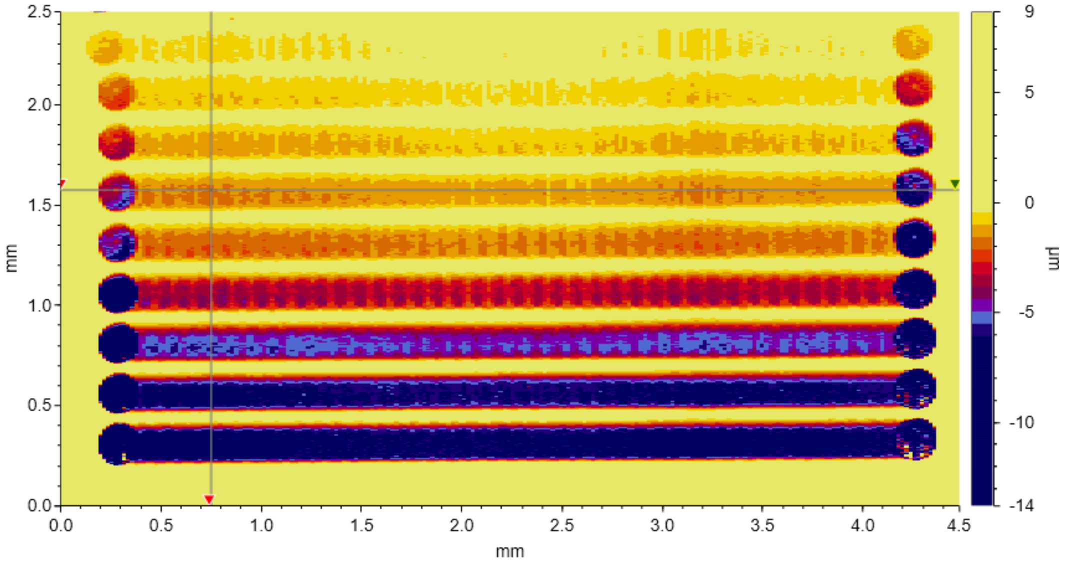

Figure A.8.: profilometric measurement of PI3; craters were obtained from LA-ICP-MS measurements; the number of pulses per crater were (from top to bottom): 1, 2, 3, 4, 5, 10, 15, 20, 25

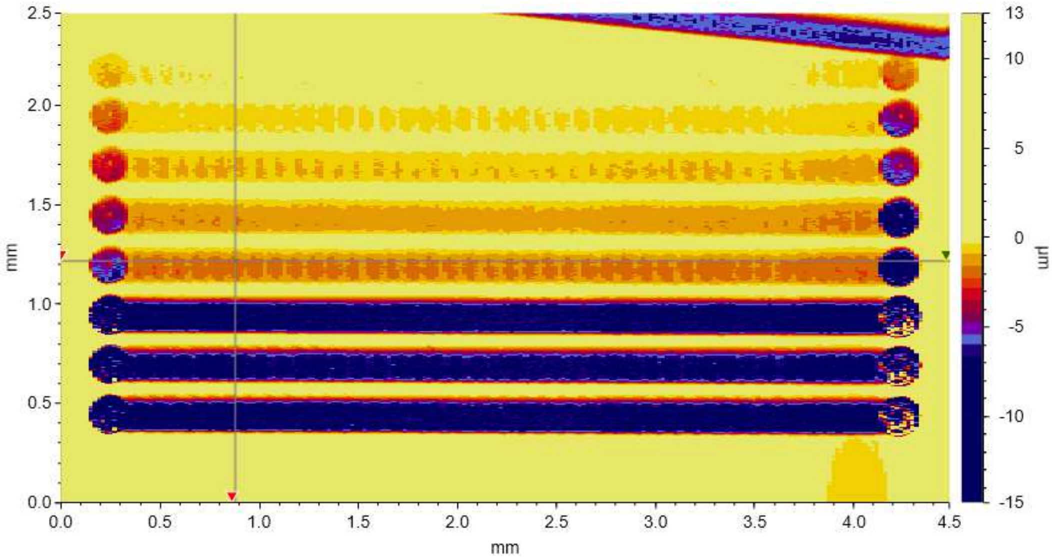

Figure A.9.: profilometric measurement of PI4; craters were obtained from LA-ICP-MS measurements; the number of pulses per crater were (from top to bottom): 1, 2, 3, 4, 5, 15, 20, 25; crater formed by 10 pulses was unintentionally left out here

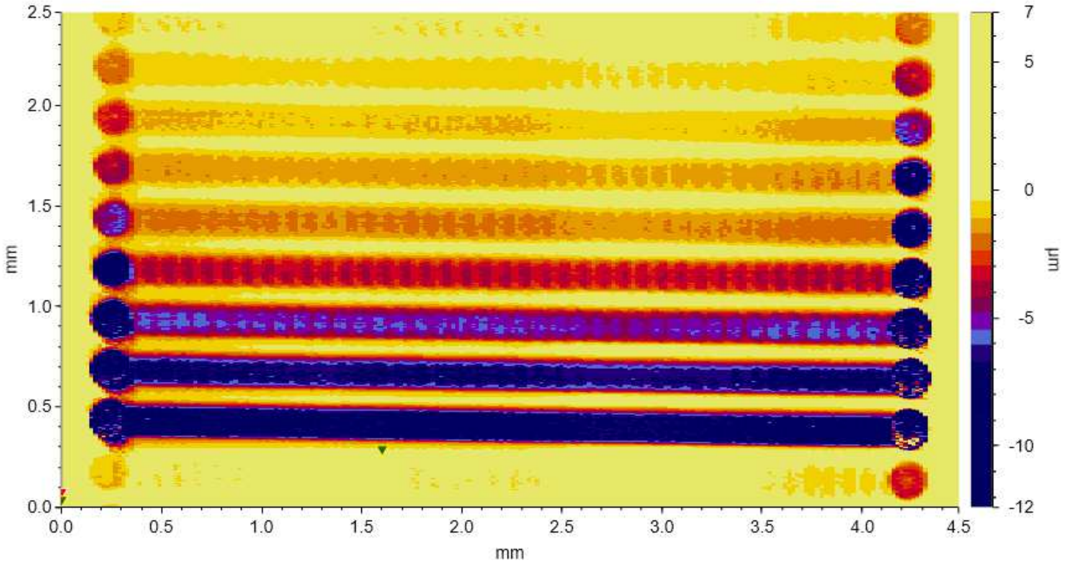

Figure A.10.: profilometric measurement of PI5; craters were obtained from LA-ICP-MS measurements; the number of pulses per crater were (from top to bottom): 1, 2, 3, 4, 5, 10, 15, 20, 25, failed

Bibliography

Aastrup, T et al. (2000). “In Situ Studies of the Initial Atmospheric Corrosion of Copper Influence of Humidity, Sulfur Dioxide, Ozone, and Nitrogen Dioxide.” In: *Journal of The Electrochemical Society* 147.7, p. 2543. ISSN: 00134651. DOI: `10.1149/1.1393566` (cit. on p. 5).

Ambat, Rajan, Stine G. Jensen, and Per Moller (2008). “Corrosion Reliability of Electronic Systems.” In: pp. 17–28. DOI: `10.1149/1.2900650` (cit. on p. 1).

American Society for Testing and Material (ASTM) (1997). “Standard Practice for Conducting Mixed Flowing Gas (MFG) Environmental Tests.” In: *American Society for Testing and Material* i, pp. 1–9. DOI: `10.1520/B0827-97` (cit. on p. 1).

American Society for Testing and Material (ASTM) (2003). “B845-97: Standard Guide for Mixed Flowing Gas (MFG) Tests for Electrical Contacts.” In: *American Society for Testing and Material* (cit. on pp. 5, 7).

Bandura, Dmitry R, Vladimir I Baranov, and Scott D Tanner (2001). “Reaction chemistry and collisional processes in multipole devices for resolving isobaric interferences in ICP–MS.” In: *Fresenius' journal of analytical chemistry* 370.5, pp. 454–470. ISSN: 0937-0633 (cit. on p. 28).

Beauchemin, D. (2014). “Inductively Coupled Plasma Mass Spectrometry Methods.” In: *Encyclopedia of Spectroscopy and Spectrometry*, pp. 236–245. DOI: `10.1016/b978-0-12-409547-2.11222-3` (cit. on pp. 21, 22, 26).

Bishop, David P et al. (2016). “Elemental bio-imaging using laser ablation-triple quadrupole-ICP-MS.” In: *Journal of Analytical Atomic Spectrometry* 31.1, pp. 197–202 (cit. on p. 27).

Bonta, Maximilian and Andreas Limbeck (2018). “Metal analysis in polymers using tandem LA-ICP-MS/LIBS: eliminating matrix effects using multivariate calibration.” In: *Journal of Analytical Atomic Spectrometry* 33.10, pp. 1631–1637. ISSN: 13645544. DOI: `10.1039/c8ja00161h` (cit. on p. 29).

Braun, Dietrich et al. (2012). *Polymer synthesis: theory and practice: fundamentals, methods, experiments*. Springer Science & Business Media. ISBN: 3642289800 (cit. on p. 8).

Chapman, John Robert and John Robert Chapman (1995). *Practical organic mass spectrometry: a guide for chemical and biochemical analysis*. John Wiley & Sons. ISBN: 047195831X (cit. on p. 24).

Chirinos, Jose R et al. (2014). "Simultaneous 3-dimensional elemental imaging with LIBS and LA-ICP-MS." In: *Journal of Analytical Atomic Spectrometry* 29.7, pp. 1292–1298 (cit. on pp. 28, 29).

Crank, John (1975). *The mathematics of diffusion*. Oxford university press. ISBN: 0198534116 (cit. on p. 10).

Cremers, David and Leon Radziemski (2013). *Handbook of Laser-Induced Breakdown Spectroscopy*. 2nd ed. Wiley Online Library, p. 432. ISBN: 9781119971122. DOI: `10.1002/9781118567371` (cit. on pp. 11–13, 15, 18, 19).

Domininghaus, Hans et al. (2008). *Kunststoffe: Eigenschaften und Anwendungen*. Series: VDI-Buch. Berlin, Heidelberg. ISBN: 978-3-540-72400-1. DOI: `10.1007/978-3-540-72401-8` (cit. on p. 8).

Dong, Meirong et al. (2015). "Elemental analysis of coal by tandem laser induced breakdown spectroscopy and laser ablation inductively coupled plasma time of flight mass spectrometry." In: *Spectrochimica Acta - Part B Atomic Spectroscopy* 109, pp. 44–50. ISSN: 05848547. DOI: `10.1016/j.sab.2015.04.008`. URL: `http://dx.doi.org/10.1016/j.sab.2015.04.008` (cit. on p. 29).

DuPont (2017). *Dupont^{TM} kapton® - summary of properties*. Tech. rep. E.I. du Pont de Nemours and Company, p. 20 (cit. on pp. 8, 9).

Dyar, M. Darby et al. (2011). "Strategies for Mars remote Laser-Induced Breakdown Spectroscopy analysis of sulfur in geological samples." In: *Spectrochimica Acta - Part B Atomic Spectroscopy* 66.1, pp. 39–56. ISSN: 05848547. DOI: `10.1016/j.sab.2010.11.016`. URL: `http://dx.doi.org/10.1016/j.sab.2010.11.016` (cit. on pp. 19, 20).

European Environmental Agency (EEA) (2018). *Air quality in Europe — 2018 report*. 5, pp. 1–64. ISBN: 9789292137021. DOI: `10.2800/62459`. URL: `papers2://publication/uuid/1D25F41B-C673-4FDA-AB71-CC5A2AD97FDD` (cit. on p. 5).

Felder, R M, C J Patton, and W J Koros (1981). "Dual-mode sorption and transport of sulfur dioxide in kapton polyimide." In: *Journal of Polymer*

Science: Polymer Physics Edition 19.12, pp. 1895–1909. ISSN: 1542-9385. DOI: 10.1002/pol.1981.180191208. URL: http://dx.doi.org/10.1002/pol.1981.180191208 (cit. on p. 10).

Freeman, B D (2010). *Membrane gas separation*. Hoboken, NJ : Wiley, 1 online resource (394 p.) ISBN: 1-119-95658-7 (cit. on pp. 9, 10).

Galazka, Rafał (2011). "MODERN ANALYTICAL METHODS IN ENVIRONMENTAL ANALYSIS – ICP-MS TECHNIQUE." In: (cit. on p. 23).

Giussani, Barbara, Damiano Monticelli, and Laura Rampazzi (2009). "Role of laser ablation–inductively coupled plasma–mass spectrometry in cultural heritage research: a review." In: *Analytica Chimica Acta* 635.1, pp. 6–21. ISSN: 0003-2670 (cit. on p. 25).

Gondal, M. A. et al. (2012). "Detection of sulfur in the reinforced concrete structures using a dual pulsed LIBS system." In: *Optics and Laser Technology* 44.3, pp. 566–571. ISSN: 00303992. DOI: 10.1016/j.optlastec.2011.09.001. URL: http://dx.doi.org/10.1016/j.optlastec.2011.09.001 (cit. on p. 20).

Grundmeier, G, W Schmidt, and M Stratmann (2000). "Corrosion protection by organic coatings: electrochemical mechanism and novel methods of investigation." In: *Electrochimica Acta* 45.15-16, pp. 2515–2533. ISSN: 0013-4686 (cit. on p. 2).

Guenther, Detlef and Bodo Hattendorf (2005). "Solid sample analysis using laser ablation inductively coupled plasma mass spectrometry." In: *TrAC Trends in Analytical Chemistry* 24.3, pp. 255–265. ISSN: 0165-9936 (cit. on pp. 15, 21, 22).

Hill, Steve J, Andrew Fisher, and Michael Foulkes (2007). "Basic Concepts and Instrumentation for Plasma Spectrometry." In: *Inductively Coupled Plasma Spectrometry and its Applications*. John Wiley & Sons, Ltd. Chap. 3, pp. 61–97. ISBN: 9780470988794. DOI: 10.1002/9780470988794.ch3. URL: https://onlinelibrary.wiley.com/doi/abs/10.1002/9780470988794.ch3 (cit. on pp. 27, 28).

Ho, P S et al. (1985). "Chemical bonding and reaction at metal/polymer interfaces." In: *Journal of Vacuum Science & Technology A: Vacuum, Surfaces, and Films* 3.3, pp. 739–745. ISSN: 0734-2101 (cit. on p. 2).

Huheey, E A (1997). *Inorganic Chemistry: Principles of Structures and Reactivity*. 4th ed. Harper Collins College (cit. on pp. 26, 61).

Jacobsen, John Bjerregaard et al. (2014). "Climate-protective packaging: Using basic physics to solve climatic challenges for electronics in demanding applications." In: *IEEE Industrial Electronics Magazine* 8.3, pp. 51–59. ISSN: 19324529 (cit. on p. 1).

Koch, J and D Günther (2007). "Femtosecond laser ablation inductively coupled plasma mass spectrometry: achievements and remaining problems." In: *Analytical and Bioanalytical Chemistry* 387.1, pp. 149–153. ISSN: 1618-2650. DOI: `10.1007/s00216-006-0918-z`. URL: `https://doi.org/10.1007/s00216-006-0918-z` (cit. on p. 13).

Koros, W J et al. (1980). "Kinetics and equilibria of sulfur dioxide sorption in kapton polyimide." In: *Journal of Polymer Science: Polymer Physics Edition* 18.7, pp. 1485–1495. ISSN: 0098-1273 (cit. on p. 10).

Kraftschik, Brian E (2013). "Advanced crosslinkable polyimide membranes for aggressive sour gas separations." PhD thesis. Georgia Institute of Technology (cit. on p. 10).

Krasniker, R., V. Bulatov, and I. Schechter (2001). "Study of matrix effects in laser plasma spectroscopy by shock wave propagation." In: *Spectrochimica Acta - Part B Atomic Spectroscopy* 56.6, pp. 609–618. ISSN: 05848547. DOI: `10.1016/S0584-8547(01)00194-X` (cit. on p. 19).

Krasniker, Rivie, Valery Bulatov, and Israel Schechter (2001). "Study of matrix effects in laser plasma spectroscopy by shock wave propagation." In: *Spectrochimica Acta Part B: Atomic Spectroscopy* 56.6, pp. 609–618. ISSN: 0584-8547 (cit. on p. 19).

Laeter, John R de et al. (2003). "Atomic weights of the elements. Review 2000 (IUPAC Technical Report)." In: *Pure and applied chemistry* 75.6, pp. 683–800. ISSN: 1365-3075 (cit. on p. 26).

Leygarf, Christofer (2016). *Atmospheric Corrosion THE ELECTROCHEMICAL SOCIETY SERIES*. ISBN: 9781118762271 (cit. on pp. 1, 4–6).

Limbeck, Andreas et al. (2015). "Recent advances in quantitative LA-ICP-MS analysis: Challenges and solutions in the life sciences and environmental chemistry ABC Highlights: Authored by Rising Stars and Top Experts." In: *Analytical and Bioanalytical Chemistry* 407.22, pp. 6593–6617. ISSN: 16182650. DOI: `10.1007/s00216-015-8858-0` (cit. on pp. 14, 15).

Ludwig, Elke (2014). "Development of ICP-based methods for quantification of sulfur in electro-deposited copper samples." PhD thesis. Vienna University of Technology, p. 73 (cit. on p. 69).

Madani, M M, H L Vedage, and R D Granata (1997). "Evaluation of polyimide coatings integrity by positron annihilation lifetime spectroscopy and electrochemical impedance spectroscopy." In: *Journal of the Electrochemical Society* 144.9, pp. 3293–3298. ISSN: 0013-4651 (cit. on p. 2).

Matsui, Shigetoshi, Takayuki Ishiguro, et al. (1997). "Effect of ultraviolet light irradiation on gas permeability in polyimide membranes. 1. Irradiation with low pressure mercury lamp on photosensitive and nonphotosensitive membranes." In: *Journal of Polymer Science Part B: Polymer Physics* 35.14, pp. 2259–2269. ISSN: 0887-6266 (cit. on pp. 10, 65).

Matsui, Shigetoshi and Tsutomu Nakagawa (1998). "Effect of ultraviolet light irradiation on gas permeability in polyimide membranes. II. Irradiation of membranes with high-pressure mercury lamp." In: *Journal of applied polymer science* 67.1, pp. 49–60. ISSN: 0021-8995 (cit. on p. 65).

Miles, Douglas L and Jennifer M Cook (2007). "Geological Applications of Plasma Spectrometry." In: *Inductively Coupled Plasma Spectrometry and its Applications*. John Wiley & Sons, Ltd. Chap. 9, pp. 277–337. ISBN: 9780470988794. DOI: `10.1002/9780470988794.ch9`. URL: `https://onlinelibrary.wiley.com/doi/abs/10.1002/9780470988794.ch9` (cit. on p. 25).

Musazzi, Sergio and Umberto Perini, eds. (2014). *Laser-Induced Breakdown Spectroscopy (Springer Series in Optical Sciences Book 182)*. 2014 editi. Springer Berlin Heidelberg, p. 565. ISBN: 9783642450846. DOI: `10.1007/978-3-642-45085-3`. arXiv: `arXiv:1011.1669v3` (cit. on pp. 11–13, 15–20).

Mushtaq, Nafeesa et al. (Mar. 2016). *Organosoluble and high Tg polyimides from asymmetric diamines containing N-amino and N-aminophenyl naphthalimide moieties*. Vol. 6. DOI: `10.1039/C6RA00143B` (cit. on p. 9).

O'Connor, Gavin and E Hywel Evans (2007). "Fundamental Aspects of Inductively Coupled Plasma–Mass Spectrometry (ICP–MS)." In: *Inductively Coupled Plasma Spectrometry and its Applications*. John Wiley & Sons, Ltd. Chap. 5, pp. 134–159. ISBN: 9780470988794. DOI: `10.1002/9780470988794.ch5`. URL: `https://onlinelibrary.wiley.com/doi/abs/10.1002/9780470988794.ch5` (cit. on pp. 23–25).

Orazio, Svelto (2010). *Principles of Laser*. 5th ed. Springer Science & Business Media, p. 625. ISBN: 9783527319978. DOI: `10.1016/B978-0-323-04332-8.00007-X` (cit. on pp. 10–12).

Osenbach, John W. (1996). "Corrosion-induced degradation of microelectronic devices." In: *Semiconductor Science and Technology* 11.2, pp. 155–162. ISSN: 02681242. DOI: `10.1088/0268-1242/11/2/002` (cit. on pp. 1, 3).

Pérez León, Carmen (Nov. 2005). "Vibrational spectroscopy of photosensitizer dyes for organic solar cells." PhD thesis (cit. on p. 18).

Pisonero, Jorge and Detlef Günther (2008). "Femtosecond laser ablation inductively coupled plasma mass spectrometry: fundamentals and capabilities for depth profiling analysis." In: *Mass spectrometry reviews* 27.6, pp. 609–623. ISSN: 0277-7037 (cit. on p. 2).

Pouli, P et al. (2005). "Measuring the thickness of protective coatings on historic metal objects using nanosecond and femtosecond laser induced breakdown spectroscopy depth profiling." In: *Spectrochimica Acta Part B: Atomic Spectroscopy* 60.7-8, pp. 1163–1171. ISSN: 0584-8547 (cit. on p. 2).

Prohaska, Thomas, Christopher Latkoczy, and Gerhard Stingeder (1999). "Precise sulfur isotope ratio measurements in trace concentration of sulfur by inductively coupled plasma double focusing sector field mass spectrometry." In: *Journal of Analytical Atomic Spectrometry* 14.9, pp. 1501–1504. ISSN: 1364-5544 (cit. on pp. 26, 27).

Safi, A. et al. (2018). "Multivariate calibration in Laser-Induced Breakdown Spectroscopy quantitative analysis: The dangers of a 'black box' approach and how to avoid them." In: *Spectrochimica Acta - Part B Atomic Spectroscopy* 144, pp. 46–54. ISSN: 05848547. DOI: `10.1016/j.sab.2018.03.007` (cit. on p. 19).

Samie, Farid et al. (2007). "Atmospheric Corrosion Effects of HNO3 A Comparison of Laboratory and Field Exposed Copper, Zinc, and Carbon Steel." In: *Journal of the Electrochemical Society* 154.5, pp. C249–C254. ISSN: 0013-4651 (cit. on p. 6).

Schweitzer, Philip A (1999). *Atmospheric degradation and corrosion control*. Vol. 12. CRC Press. ISBN: 0824777093 (cit. on pp. 3, 4).

Sharp, Barry L and Ciaran O'Connor (2007). "Aerosol Generation and Sample Transport." In: *Inductively Coupled Plasma Spectrometry and its Applications*. John Wiley & Sons, Ltd. Chap. 4, pp. 98–133. ISBN: 9780470988794. DOI: `10.1002/9780470988794.ch4`. URL: `https://onlinelibrary.wiley.com/doi/abs/10.1002/9780470988794.ch4` (cit. on p. 22).

Siegman, A. E. (1986). *Lasers*. University Science Books, p. 1304 (cit. on p. 10).

Skoog, Douglas A, F James Holler, and Stanley R Crouch (2017). *Principles of instrumental analysis*. Cengage learning. ISBN: 1305577213 (cit. on pp. 17, 23–25).

Syta, Olga et al. (2018). "Elemental imaging of heterogeneous inorganic archaeological samples by means of simultaneous laser induced breakdown spectroscopy and laser ablation inductively coupled plasma mass spectrometry measurements." In: *Talanta* 179.December 2017, pp. 784–791. ISSN: 00399140. DOI: 10.1016/j.talanta.2017.12.011 (cit. on p. 29).

Tidblad, Johan et al. (2017). "ICP materials trends in corrosion, soiling and air pollution (1987-2014)." In: *Materials* 10.8. ISSN: 19961944. DOI: 10.3390/ma10080969 (cit. on p. 6).

Tummala, Rao R, Eugene J Rymaszewski, and Alan G Klopfenstein (2012). *Microelectronics packaging handbook: technology drivers*. Springer Science & Business Media. ISBN: 1461540860 (cit. on p. 2).

Valdez Salas, Benjamin et al. (2013a). "Copper Corrosion by Atmospheric Pollutants in the Electronics Industry." In: *ISRN Corrosion* 2013.X, pp. 1–7. ISSN: 2090-8903. DOI: 10.1155/2013/846405. URL: http://www.hindawi.com/journals/isrn.corrosion/2013/846405/ (cit. on p. 1).

Valdez Salas, Benjamin et al. (2013b). "Copper Corrosion by Atmospheric Pollutants in the Electronics Industry." In: *ISRN Corrosion* 2013, pp. 1–7. DOI: 10.1155/2013/846405 (cit. on p. 5).

Van Malderen, Stijn J M, Johannes T van Elteren, and Frank Vanhaecke (2015). "Development of a fast laser ablation-inductively coupled plasma-mass spectrometry cell for sub-μm scanning of layered materials." In: *Journal of Analytical Atomic Spectrometry* 30.1, pp. 119–125 (cit. on p. 22).

Vonderheide, Anne P et al. (2007). "Environmental and Clinical Applications of Inductively Coupled Plasma Spectrometry." In: *Inductively Coupled Plasma Spectrometry and its Applications*. John Wiley & Sons, Ltd. Chap. 10, pp. 338–386. ISBN: 9780470988794. DOI: 10.1002/9780470988794.ch10. URL: https://onlinelibrary.wiley.com/doi/abs/10.1002/9780470988794.ch10 (cit. on p. 25).

World Health Organization (WHO) (2000). *Air Quality Guidelines*. Vol. 2. World (cit. on pp. 5, 6).

Yeh, J T C (1986). "Laser ablation of polymers." In: *Journal of Vacuum Science & Technology A: Vacuum, Surfaces, and Films* 4.3, pp. 653–658. ISSN: 0734-2101 (cit. on p. 2).

Yi, Honghong et al. (2012). "Adsorption equilibrium and kinetics for SO2, NO, CO2 on zeolites FAU and LTA." In: *Journal of hazardous materials* 203, pp. 111–117. ISSN: 0304-3894 (cit. on p. 10).

Zakipour, S, J Tidblad, and C Leygraf (1995). "Atmospheric corrosion effects of SO2 and O3 on laboratory-exposed copper." In: *Journal of the Elec-*

trochemical Society 142.3, pp. 757–760. ISSN: 00134651. DOI: 10.1149/1.2048530. URL: http://www.scopus.com/inward/record.url?eid=2-s2.0-0029273838%7B%5C&%7DpartnerID=40%7B%5C&%7Dmd5=efc90bc4d5fb74f9c3d126ae27f4ee1b (cit. on p. 5).

Zakipour, S, J Tidblad, and C Leygraf (1997). "Atmospheric Corrosion Effects of SO 2, NO 2, and O 3 A Comparison of Laboratory and Field Exposed Nickel." In: *Journal of the Electrochemical Society* 144.10, pp. 3513–3517. ISSN: 0013-4651 (cit. on p. 6).